Theory of finite periodic systems: General expressions and various simple and illustrative examples

Pedro Pereyra[1,2] and Edith Castillo[1,3]
[1]*Departamento de Ciencias Básicas, UAM-Azapotzalco, Av. S. Pablo 180, C.P. 02200, México*
[2]*The Abdus Salam International Center for Theoretical Physics, Trieste, Italy*
[3]*Departamento de Física, Universidad de Guadalajara, Guadalajara 44100, Jalisco, México*
(Received 26 June 2001; revised manuscript received 1 February 2002; published 20 May 2002)

A comprehensive presentation of an approach to finite periodic systems is given. The general expressions obtained here allow simple and precise calculations of various physical quantities characteristic of crystalline systems. Transmission amplitudes through *n*-cell *multichannel* quantum systems are rigorously derived. General expressions for several physical quantities are entirely expressed in terms of single-cell amplitudes and a new class of polynomials $p_{N,n}$. Besides the general expressions, we study some superlattice properties such as the band structure and its relation to the phase coherence phenomena, the level density and the Kronig-Penney model as its continous espectrum limit. Band structure tailoring, optical multilayer systems, resonant energies and functions, and channel-mixing effects in multichannel transport processes are also analyzed in the light of this approach.

DOI: 10.1103/PhysRevB.65.205120 PACS number(s): 71.15.−m, 71.10.−w, 71.20.−b, 72.10.−d

I. INTRODUCTION

The solid-state theory that has evolved into the present condensed matter physics carries a burden of prequantic theoretical tools to describe periodic systems. In the current theory, the reciprocal space and its corresponding methods (appropriate and natural to deal with Miller indices and structural analysis of crystalline materials) were, so to say, customized for a quantum description of periodic systems. Simultaneously, the translational invariance and the ensuing Bloch's theorem,[1] rigorously valid only for *infinite* periodic systems, become the natural and obvious starting point to deal with real periodic systems which, although macroscopic, are *finite*. Despite the important results obtained and the great amount of interesting phenomena that have been explained so far,[2,3] the theoretical analysis in the reciprocal space provides a rather involved and sometime obscure description of the physics of the crystalline systems. An alternative approach, which is much simpler and natural for studying finite periodic systems, without any reference to Bloch's theorem or reciprocal spaces, was recently introduced.[4] Further developments and details of this theory will be presented here. In this approach, which relies on simple algebraic methods and was envisioned to study systems with an arbitrary number of cells, an arbitrary number of propagating modes and an arbitrary shape of single-cell-potential, exact, and general expressions can be determined for quantities which are either impossible to calculate within the present theory or may require experimental input.

This theory follows a procedure which is in some sense similar to the one used in solving simple quantum mechanical problems such as the square well potential, the harmonic oscillator, etc. In these cases the energy eigenvalues and the eigenfunctions are directly obtained without any reference to reciprocal spaces or approximate methods. As will be seen in this paper and forthcoming publications, an appropriate use of the transfer matrix properties allows one to study finite periodic systems and to rigorously deduce analytical and general expressions for a number of physical quantities characterizing open and bounded systems. In the present approach and in the traditional solid-state physics theory, the way in which the periodicity and finiteness of the systems are incorporated in the theory is handled differently and the extent and limitations of the theoretical predictions dependent on how this problem is confronted. In the traditional approach,[1–11] the translational invariance is assumed from the very beginning and leads to the widely accepted Bloch functions $e^{ik_B\cdot r}u_{\mu,k_B}(r)$, where the periodic part $u_{\mu,k_B}(r)$ remains practically unknown or approximately determined by rather involved numerical calculations. This function is taken as a rigorous solution of the Schrödinger equation, which is *not* true unless the size of the system is taken to be infinite. This underlying assumption implies that the current theory stays in the continuous spectrum limit and draws one in a very natural way to work and develop a theory in the reciprocal space. A number of well-established but approximate methods have been developed to basically evaluate dispersion relations at different symmetry points of the Brillouin zone. In the transfer-matrix approach on the other hand, (local) periodicity and finiteness, inherent to the theory, are fully introduced without any drawback, and a theory of finite periodic systems is neatly built up on them. Universal expressions for global *n*-cell physical quantities, valid for any realization of the potential function, are rigorously and directly obtained in our theory. We believe that in some cases the transfer matrix approach will substitute with advantage the current models, while in other cases, but not in general, an appropriate combination will work better.

In the standard approaches to multilayer systems both the transverse translational invariance and the one-dimensional (1D) one-channel (or propagating mode) approximations are regularly invoked. These convenient assumptions stand up, whereas channel mixings are negligible. Otherwise, it is not possible to sustain the 1D one-channel assumption when a real multimode propagation process is present. A theory where a multichannel approach is possible is then required. In general, even at low energies and for narrow systems a number of propagating modes (*open physical channels*)

might be present. In the scattering approach to electronic transport processes, each of the transverse nonevanescent states in the leads define an open channel. For a 2D system—say, an electron gas in a GaAs layer with transverse width w and energy E—the number of (electron) propagating modes is of the order of $2w\sqrt{2m^*E}/\pi\hbar \approx 0.8w\sqrt{E}$. For $w \simeq 8$ nm and $E \gtrsim 0.1$ eV this number is $N \approx 2$. We shall in general conceive the physical channels in a wider sense. Hence, light and heavy holes or any other propagating mode can be considered as a concrete realization of a channel.

In the theory of finite periodic systems (TFPS's) discussed here and in the forthcoming parts, the finiteness property of real systems and the possibility of multichannel processes are essential to the theory and they are explicitly built in. In this theory we use the more suitable transfer-matrix method, which, although scarcely used in solving quantum mechanical problems, provides an extremely powerful technique, mathematically simple, and, from the point of view of the physical results, fairly appealing and significant.

The possibility of easy derivations of general expressions to describe the physics of the whole n-cell system is an important advantage of this approach. Some highly remarkable characteristics of these expressions are their simplicity and compactness. The fundamental properties of the quantum description such as the *tunneling effect* and *phase coherence phenomena* are evident in their functional structure. Just to illustrate what we mean here, let us refer to the n-cell N-channel transmission amplitude $t_{N,n}$ obtained in Eq. (27), where for simplicity the subindex N has been dropped. This global quantity is a simple function of the one-cell transmission t $(=t_{N,1})$ amplitude and certain well-defined polynomials p_n $(=p_{N,n})$. In that expression, t carries information on the tunneling process while p_n on the phase coherence phenomena. In the 1D (one channel) case, p_n reduces to the well-known Chebyshev polynomial of the second kind U_n.

In the theory of finite periodic systems, the polynomials $p_{N,n}$ comprise the whole information of the *complicated phase interference processes*, originating in the multiple reflections along the ''periodic'' system, and of the system's size L $(=nl_c$ in the growing direction) reflected in the order of the polynomial. The multichannel polynomials $p_{N,n}$ are interesting quantities not only from the point of view of the physics but also from that of the mathematics. Physical properties that are strongly determined by quantum coherence and tunneling effects, such as the resonant transmission behavior and the energy band structure, are thoroughly settled out by the single-cell transfer matrix and the number of cells, n. It is worth mentioning that all the results in this theory are compatible and reduce, when taking appropriate limits, to well-known physical properties and expressions.[12–19] In this theory, even the popular and illustrative Kronig-Penney (KP) model can be derived in a more natural and simple way.

In this paper we shall refer mainly to multichannel time-reversal-invariant and -noninvariant systems with and without spin-dependent interactions, i.e., to systems of the so-called orthogonal, symplectic, and unitary universality classes, named by the kind of matrix that diagonalizes the Hamiltonian H, respectively.[20] Since the most general or less restrictive class of systems is those of the unitary universality class (with time reversal symmetry broken and, depending, or not, on the spin), most of the expressions derived in this part will refer to this kind of system. However, in some cases we will be more specific with the universality classes. For the sake of simplicity we will discuss examples of the orthogonal class, i.e., spin-independent and time-reversal-invariant systems.

The TFPS's will be discussed in three parts. In the first part, we will introduce the transfer-matrix method, establish general properties using the scattering amplitudes, and deduce general expressions for the evaluation of a number of physical quantities in open systems. In the second part we will refer to bounded and quasibounded systems and the intraband energy eigenvalues and eigenfunctions. In the third part we will apply the results obtained to the calculation of the band structure for real systems, such as GaAs and AlAs, taking into account the e-e and e-nucleus Coulomb interactions, the repulsive angular potential, and the spin-orbit interaction.

In Sec. II, of this first part, we shall present an overview of the transfer-matrix definition and recall the well-known relations with the scattering amplitudes. In Sec. II B, we derive a general three-term recurrence relation, which is an important piece of the theory, whose solutions are the matrix polynomial $p_{N,n}$. In Sec. III, new and general expressions for the scattering amplitudes and the associated n-cell transport quantities are derived. Closed and compact expressions for an easy evaluation of the resonant energies and resonant functions of open systems are also presented. Since all these quantities are shown to depend on the polynomials $p_{N,n}$, we present in Sec. IV, for completeness and self-consistency, an outline of the solution of the three-term recurrence relation obtained in Ref. 21. In Sec. V, 1D one channel and 3D multichannel examples are discussed.

To illustrate the application of the theory to one-channel periodic systems, we shall consider the typical square- and δ-barrier potential chains. Various well-known properties such as the band structure, resonant tunneling probabilities, transmission coefficients, resonant energies, and wave functions will be calculated. Level densities, including the interesting coherence-induced localization effect in open systems, will also be disscused. The interesting and well-known band structure ''tailoring'' and the familiar energy levels and subbands in the gap regions are also nicely accounted for by adding ''impurities'' or producing topological defects to the finite periodic systems. Concerning the multichannel systems, and to exhibit the advantages of this formalism when dealing with channel mixings, we will finally include some examples of two and three propagating modes through alternating thick GaAs layers and thin films of δ-repulsive or δ-attractive centers, with interesting resonance effects arising from phase coherence, channels coupling, or coupling between an open and an evanescent mode.

Since the principal results of this paper are equally valid for electromagnetic systems, evaluation of optical transmission properties through optical multilayer heterostructures is also possible. The superluminal tunneling time through optical superlattices[22] or the nonlinear multilayer optical arrays

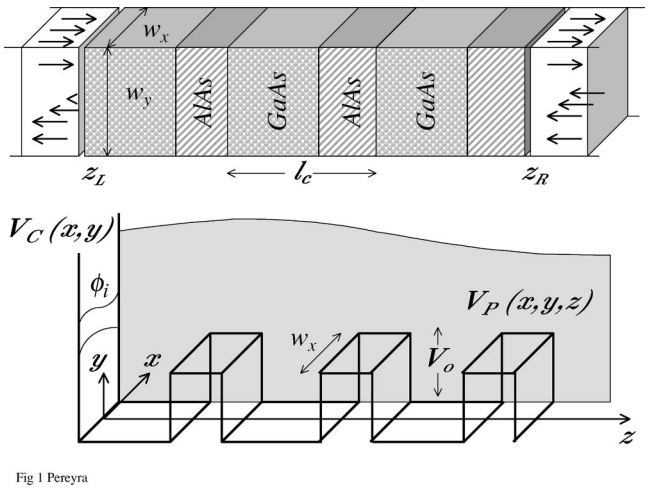

Fig 1 Pereyra

FIG. 1. Particles moving through a 3D superlattice of lateral dimensions w_x, w_y and cell length l_c feel a lateral confining hard-wall potential $V_C(x,y)$ and a periodic potential V_P, at least as a function of the growing coordinate z.

with alternating ''dielectric constants''[23] in the ''single-layer approximation'' have been also successfully attacked. For the last case we shall calculate the transmission coefficients and the optical band structure.

II. TRANSFER-MATRIX APPROACH FOR MULTICHANNEL FINITE PERIODIC SYSTEMS

A. Properties, definitions, and the scattering amplitudes

Transfer matrices and their properties were used in the 1950s as natural quantities to describe electronic spectra and transport processes through ordered and disordered linear chains.[24,25] More recently, multichannel-transfer-matrix approaches became familiar in the scattering theory of quantum wires.[26] Basically two types of transfer matrices are known: the transfer matrix (which we shall call of the first kind), which connects *wave functions and their derivatives at two points or planes of the scattering region*, and the transfer matrix (of the second kind), which relates the *state vectors at those points or planes*. Transfer matrices of the first kind were used by James[24] and quite recurrently in 1D solid-state physics.[25] On the other hand, the matrices of the second kind were used by Luttinger[27] and Borland,[28] who denoted them ''transformation matrices.'' Lately, matrices of this type have appeared somehow more frequently and came to be also called ''transfer matrices.'' Both types of transfer matrices can, of course, be related to each other by a simple transformation. In this paper we will be concerned with transfer matrices of the second kind relating state vectors.

If we were dealing with an electronic transport process through a 3D ''periodic'' system (of length $l=z_R-z_L$ and transverse cross section $w_x w_y$) connected to perfect leads (or waveguides) of equal cross section (see Fig. 1), the assumed noninteracting charge carriers would feel a potential function containing at least a confining hard wall potential $V_C(x,y)$ and a periodic potential $V_P(x,y,z)$, periodic at least as a function of one coordinate—say, the coordinate z. Solving the partial differential equation

$$-\frac{\hbar^2}{2m}\left(\frac{\partial^2}{\partial x^2}+\frac{\partial^2}{\partial y^2}\right)\phi_{n_x n_y}+V_C(x,y)\phi_{n_x n_y}=E_{n_x n_y}\phi_{n_x n_y}, \tag{1}$$

a set of functions $\phi_{n_x n_y}(x,y)$ and physical channels can be defined in the leads. For a given Fermi energy E, a number of open channels or propagating modes with threshold energies

$$E_i=\frac{\hbar^2\pi^2}{2m}\left(\frac{n_x^2}{w_x^2}+\frac{n_y^2}{w_y^2}\right)\leqslant E \tag{2}$$

can be identified. Notice that all the possible physical states can be labeled by a channel index $i=\{n_x,n_y\}=1,2,\ldots,s\mathcal{N}$, where s is the number of spin projections (taken into account only when the interaction depends on the spin) and $\mathcal{N}$ is of the order of $(k_F w)^{D-1}$, with D the system's dimensionality and k_F the Fermi wave vector. From here on, the number of propagating modes is taken in general as $N=s\mathcal{N}$. We can use the set of functions $\{\phi_i(x,y)\}$ to express the total wave function as

$$\Psi(x,y,z)=\sum_i^N \phi_i(x,y)\varphi_i(z). \tag{3}$$

Substituting in the Schrödinger equation, we obtain the following system of coupled equations:[29]

$$\frac{d^2}{dz^2}\varphi_i(z)-(\kappa^2+k_{Ti}^2)\varphi_i(z)=\sum_j^N K_{ij}\varphi_j(z), \quad i=1,2,\ldots,N,$$

where $\kappa=\sqrt{2m(V_P-E)/\hbar}$, $k_{Ti}^2=2mE_i/\hbar^2$, and the channel coupling parameter

$$K_{ij}=\frac{2m}{\hbar^2}\int \phi_i^*(x,y)V_P(x,y,z)\phi_j(x,y)\,dx\,dy. \tag{4}$$

Although the contribution of the so-called ''closed channels'' (evanescent modes) can, in principle, be taken into account, we shall in general disregard their contribution.

To determine the transmission amplitudes from z_L to $z_R=z_L+nl_c$, where l_c is the length of a single cell, the standard procedure would require one to solve the coupled equations and match the solutions all the way from z_L to z_R. Here, with a suitable method, we only need to solve the single-cell problem to describe most of the superlattice physical properties.

Let $\vec{\varphi}_{i\sigma}(z)$ and $\overleftarrow{\varphi}_{i\sigma}(z)$ be the ith-channel (with spin σ) wave functions traveling to the right and left, respectively. The total wave functions in the left- and right-hand sides of the scattering region (see Fig. 2) can be written as

$$\varphi(z_1)=\sum_{i=1}^{\mathcal{N}}\sum_{\sigma=1}^{s}\left[a_{i\sigma}\vec{\varphi}_{i\sigma}(z_1)+b_{i\sigma}\overleftarrow{\varphi}_{i\sigma}(z_1)\right]$$

$$=(a,b)\begin{pmatrix}\vec{\varphi}(z_1)\\ \overleftarrow{\varphi}(z_1)\end{pmatrix}, \tag{5}$$

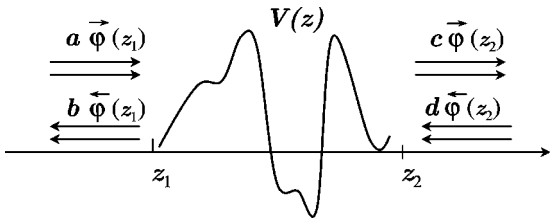

FIG. 2. Left- and right-propagating wave functions at two points z_1 and z_2 of a potential region.

$$\varphi(z_2)=\sum_{i=1}^{\mathcal{N}}\sum_{\sigma=1}^{s}\left[c_{i\sigma}\vec{\varphi}_{i\sigma}(z_2)+d_{i\sigma}\overleftarrow{\varphi}_{i\sigma}(z_2)\right]$$

$$=(c,d)\begin{pmatrix}\vec{\varphi}(z_2)\\ \overleftarrow{\varphi}(z_2)\end{pmatrix}, \tag{6}$$

where a,b,c, and d are N-dimensional coefficients. These functions, in the state vector representation, are related with each other by a transfer matrix of the second kind defined by

$$\begin{pmatrix}c\vec{\varphi}(z_2)\\ d\overleftarrow{\varphi}(z_2)\end{pmatrix}=M(z_2,z_1)\begin{pmatrix}a\vec{\varphi}(z_1)\\ b\overleftarrow{\varphi}(z_1)\end{pmatrix}. \tag{7}$$

For our purposes it is useful to express the transfer matrix in block notation as

$$M(z_2,z_1)=\begin{pmatrix}\alpha & \beta\\ \gamma & \delta\end{pmatrix}, \tag{8}$$

where α, β, γ, and δ are $s\mathcal{N}\times s\mathcal{N}$ or just $N\times N$ complex submatrices. In general, there are some constrictions between the submatrices α, β,γ, and δ, which of course depend on the physical properties and symmetries present in the system's Hamiltonian. As mentioned above, the physical systems are especially distinguished by the presence or not of time-reversal and spin-rotation symmetries. In each case, the number of free parameters and the characteristics of the transfer matrix are determined by the symmetries.[20,26]

While time reversal invariance and spin-dependent interactions (SDI's) may or may not be present, flux conservation (FC) must always hold and the transfer matrices should fulfill the pseudounitarity condition (see Appendix B)

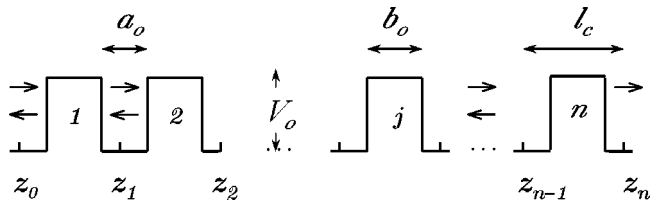

FIG. 3. One-dimensional finite periodic system of square barrier of height V_0 and width b_0, separated by valleys of width a_0.

$$M\Sigma_z M^{\dagger}=\Sigma_z,$$

$$\text{with}\quad \Sigma_z=\begin{pmatrix}I_N & 0\\ 0 & -I_N\end{pmatrix}, \tag{9}$$

where I_N is the $N\times N$ identity matrix. In the absence of time reversal invariance, the Hamiltonians for both spin-dependent and spin-independent interactions can be diagonalized by a unitary transformation; hence the system belongs to the *unitary universality class*. In the presence of time-reversal invariance (TRI), we distinguish the spin-dependent case from the spin-independent one. For spin-independent systems, of the so-called *orthogonal universality class*, time-reversal invariance implies that $\delta=\alpha^*$ and $\gamma=\beta^*$, while for spin-dependent systems, of the *symplectic universality class*, TRI implies other requirements. For spin-1/2 particles, the transfer matrices have the structure[20]

$$M_s=\begin{pmatrix}\alpha & \beta\\ k^T\beta^* k & k^T\alpha^* k\end{pmatrix},$$

$$\text{with}\quad k=\begin{pmatrix}0 & I_{\mathcal{N}}\\ -I_{\mathcal{N}} & 0\end{pmatrix}. \tag{10}$$

The specific functional form of the transfer-matrix elements depends on the particular potential functions. For the sake of illustration, let us consider here a periodic system of square barriers of height V_0 and width b_0 separated by valleys of width a_0, as shown in Fig. 3. The single-cell transfer matrix, relating wave vectors at, say, z_1 and z_2, is the well-known matrix (see Appendix A and Ref. 30)

$$M_{sb}=\begin{pmatrix}e^{ika_0}\cosh(\kappa b_0)-i\dfrac{(\kappa^2-k^2)}{2k\kappa}\sinh(\kappa b_0) & -i\dfrac{(\kappa^2+k^2)}{2k\kappa}\sinh(\kappa b_0)\\ +i\dfrac{(\kappa^2+k^2)}{2k\kappa}\sinh(\kappa b_0) & e^{-ika_0}\cosh(\kappa b_0)+i\dfrac{(\kappa^2-k^2)}{2k\kappa}\sinh(\kappa b_0)\end{pmatrix}, \tag{11}$$

with $k=\sqrt{2mE}/\hbar$ and $\kappa=\sqrt{2m(V_0-E)}/\hbar$. This system is time-reversal invariant and belongs to the orthogonal universal class. Hence $\delta=\alpha^*$ and $\gamma=\beta^*$. It is easy to verify that this matrix also fulfills the FC requirement.

Although the explicit calculation of the transfer matrix for an arbitrary potential region may not be a simple task, it is still possible to establish (based on very general transfer-matrix properties) many interesting results without any

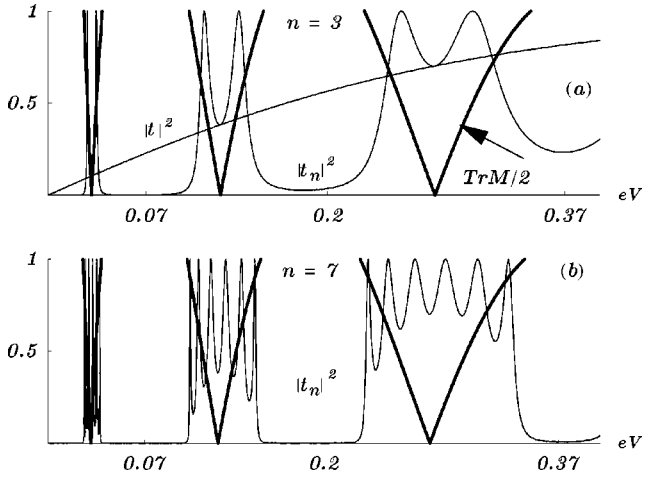

FIG. 4. In these figures the trace $\mathrm{Tr}\, M_{sb}/2$ is plotted together with the transmission coefficients $|t_n|^2$ for the periodic system in Fig. 3, with $V_0=0.23$ eV, $b_0=10$ nm, $a_0=5$ nm, and $n=3,7$ in (a) and (b), respectively. In (a) we also have the single-cell transmission coefficient $|t|^2$. It is evident from these figures that the Kramer condition $|\mathrm{Tr}\, M_0|\leqslant 2$ determines the allowed and forbidden energy regions.

reference to their explicit functional form.

At this point we shall introduce a brief digression to refer to one of the most important and relevant physical concepts of the crystalline systems: the band structure, from a transfer-matrix point of view. It is well known that in order to determine the energy regions of extended wave functions one can use Kramer's condition.[30] In the 1D one propagating mode approximation this condition is written as $|\mathrm{Tr}\, M_0|\leqslant 2$. Similar relations, appropriately modified, work well for systems with a larger number of propagating modes. For the familiar 1D Kronig-Penney model shown in Fig. 3, i.e., for the sequence of square-barrier potentials mentioned before, the single-cell transfer-matrix trace is

$$\mathrm{Tr}\, M_{sb}=2\left(\cos(ka_0)\cosh(\kappa b_0)+\frac{(\kappa^2-k^2)}{2k\kappa}\sin(ka_0)\sinh(\kappa b_0)\right). \qquad (12)$$

The right-hand-side function is frequently quoted in the literature as equal to $\cos k_{Bl}l_c$, the cosine of the Bloch phase $k_{Bl}l_c$. In Figs. 4(a) and 4(b), $\mathrm{Tr}\, M_{sb}/2$ is plotted together with the transmission coefficients, referred to below. It is evident from these figures that the Kramer condition $|\mathrm{Tr}\, M_0|\leqslant 2$ determines the band structure. In theories designed for infinite periodic systems, the allowed energy bands are continuous regions of energy levels. However, from calculations of transmission coefficients for finite periodic systems the bands contain a finite number of energy levels and the band structure manifests itself when the number of cells n is of the order of 5.

Sometimes it may be convenient, but it is not essential for this theory, to express the transfer matrices in the Bargmann's representation, briefly mentioned in Appendix B and extensively studied in Ref. 20. In this representation and for 1D systems of the orthogonal universality class, the transfer-matrix trace reduces to

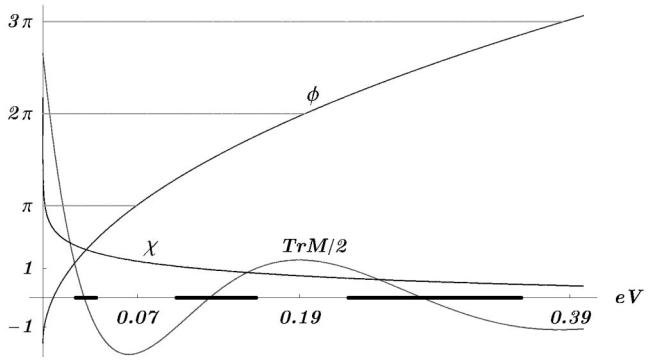

FIG. 5. The Bargmann parameters ϕ and χ and the transfer-matrix trace $\mathrm{Tr}\, M_0/2$ as functions of the energy for the periodic system in Fig. 3. The energy bands are emphasized in the energy axis. The phase ϕ is a monotonously increasing function of the energy, with an allowed energy band for each interval of length π. The parameter χ, on the other hand, decreases monotonously. These two parameters define not only the appearance of resonant states and bands but also the building up of gaps.

$$\mathrm{Tr}\, M_0=2\cos\phi\cosh\chi=2\,\mathrm{Re}\,\alpha, \qquad (13)$$

with ϕ and χ being well-defined functions of the energy and the specific potential parameters. In Fig. 5 we plot the functions ϕ and χ, together with the transfer-matrix trace $\mathrm{Tr}\, M_0/2$. The energy bands are indicated in the energy axis with bold lines. The phase ϕ is a monotonous increasing function of the energy, with an allowed energy band for each interval of length π. The parameter χ, on the other hand, decreases monotonically. These two parameters define not only the appearance of resonant states and bands but also the building up of the gaps. Note that we can label the bands with an index defined by $\mu=1+(\phi-\phi \bmod \pi)/\pi$. It is important to make clear that, even though the band structure is a consequence of and will emerge once the phase coherence and the periodicity have been combined, the single-cell transfer matrix already contains information on this fundamental property.

The Bloch's phase $\theta_{Bl}=k_{Bl}l_c$ and the Bargmann parameters are related by

$$\cos\theta_{Bl}=\cos\phi_\mu\cosh\chi, \qquad (14)$$

with $\phi_\mu=\phi \bmod \pi$. A simple analysis of this equation and the energy dependence of ϕ_μ and χ (see Fig. 5) neatly explains the reappearance of bands and gaps with varying width. It also shows that the Bloch phase θ_{Bl} comprises the behavior of the real compact and noncompact parameters ϕ and χ, respectively. As these parameters vary, the Bloch phase passes from a real value (allowed band) to an imaginary value (forbidden band).

To describe tunneling and transport properties in terms of transmission amplitudes, it is important to recall the relation between the transfer matrix M and the scattering S matrix.

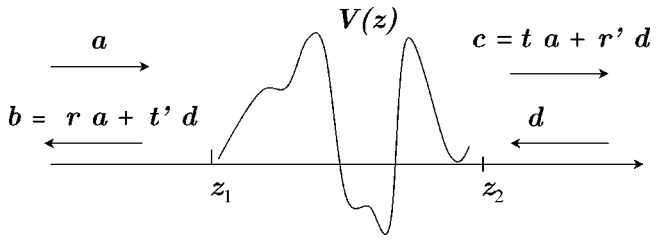

FIG. 6. The inccoming and outgoing amplitudes and the scattering amplitudes for particles coming in from the left- and right-hand sides.

For scattering processes like the one sketched in Fig. 6, the coefficients r, t, r', and t' are the reflection and transmission amplitudes corresponding to incident particles on the left- and right-hand sides, respectively. It is easy to verify (see, for example, Appendix C), that the transfer matrix of the unitary universality class can be written as

$$M_u=\begin{pmatrix}\alpha & \beta\\ \gamma & \delta\end{pmatrix}=\begin{pmatrix}(t^\dagger)^{-1} & r'(t')^{-1}\\ -(t')^{-1}r & (t')^{-1}\end{pmatrix}. \tag{15}$$

When time-reversal symmetry is conserved, one has to distinguish spin-dependent from spin-independent systems, as mentioned before. The TRI requirement for spin-independent systems implies $t'=t^T$ while for spin-dependent and TRI systems $t'=k^Tt^Tk$. Here the superscript T stands for the transpose. These global relations (valid independently of the size of the system, number of cells, and the potential profiles) are part of the cornerstone of the transfer-matrix method and they provide the possibility of establishing a bridge between the mathematically well-defined objects: the transfer matrices and the scattering amplitudes.

Another important attribute of the transfer matrices that makes them appropriate quantities to describe systems of finite but, in principle, arbitrary length is the multiplicative property

$$M(z_3,z_1)=M(z_3,z_2)M(z_2,z_1), \tag{16}$$

where $M(z_j,z_i)$ is the transfer matrix relating state vectors at positions z_i and z_j. This property and the possibility of relating the matrix with the scattering amplitudes have been broadly used; they constitute the principal ingredients of the transfer-matrix approach to the quantum description of finite periodic systems.

It is well known that, in general, the scattering and the transfer matrices contain the whole information of the scattering processes. Hence it is not surprising that based on these quantities one could build a theory to describe the physics of systems whose geometry permits the definition of the corresponding transfer matrix. To exploit this method, it is essential to improve the ability to *analytically* calculate consequences and new results associated with the transfer matrix and, hence, with the scattering amplitudes at any point of the system. This is, in principle, possible and it is the goal of the next section. We shall establish a general method and deduce general formulas that can be applied directly to determine physical quantities for specific finite periodic systems.

B. *n*-cell transfer matrix and some basic relations

The multiplicative property of transfer matrices makes them suitable quantities to describe systems whose length grows. If we put together two identical cells of length L/n and with a transfer matrix M each, the resulting system of length $2L/n$ has the transfer matrix $M_2=MM=M^2$. The physical information of the enlarged system is fully contained in the resulting transfer matrix M_2, while the functional relation of M_2 with the physical quantities (scattering amplitudes) remains unchanged. Applying the multiplicative property over and over, we can express the global (n-cell) transfer matrix as

$$M_n=M^n=\begin{pmatrix}\alpha & \beta\\ \gamma & \delta\end{pmatrix}^n\equiv\begin{pmatrix}\alpha_n & \beta_n\\ \gamma_n & \delta_n\end{pmatrix}, \tag{17}$$

which is related to the corresponding scattering amplitudes by

$$\begin{pmatrix}\alpha_n & \beta_n\\ \gamma_n & \delta_n\end{pmatrix}=\begin{pmatrix}(t^\dagger_{N,n})^{-1} & r'_{N,n}(t'_{N,n})^{-1}\\ -(t'_{N,n})^{-1}r_{N,n} & (t'_{N,n})^{-1}\end{pmatrix}. \tag{18}$$

A quite significant step in the transfer-matrix method is, precisely, the possibility of analytically determining the matrices α_n, β_n, etc., and hence, from Eq. (18), to deduce analytical expressions for the global n-cell N-channel physical quantities. The subindex N will be usually absent in the TM blocks and the one channel quantities, just for simplicity. For numerical evaluations it may be convenient to diagonalize M as $U\Lambda U^\dagger$ and to write the n-cell transfer matrix as $U\Lambda^nU^\dagger$. However, by doing this one loses all the power of the transfer-matrix method for analytical calculations and spoils the possibility of deriving new expressions for fundamental physical quantities.

Let us now consider some transfer-matrix properties and derive fundamental relations in this approach. In the following we will be concerned mainly with the unitary universality class with transfer matrix M_u, but for an easy notation the subindex u will be omitted.

Since

$$M_n=MM_{n-1}, \tag{19}$$

it is clear that

$$\alpha_n=\alpha\alpha_{n-1}+\beta\gamma_{n-1} \tag{20}$$

and similar ones for β_n, γ_n, and δ_n, with $\alpha_0=\delta_0=I_{s,N}$ and $\beta_0=\gamma_0=0$. Starting from these relations one can easily obtain the *matrix recurrence relation (MRR)*

$$\beta_n=(\alpha+\beta\delta\beta^{-1})\beta_{n-1}+(\beta\gamma-\beta\delta\beta^{-1}\alpha)\beta_{n-2}, \tag{21}$$

and a similar ones for α_n, γ_n, and δ_n. All these relations are three-term recurrence relations with matrix coefficients of dimension $N\times N$. If we define the matrix functions

$$p^{(1)}_{N,m-1}=\beta^{-1}\beta_m, \tag{22}$$

Eq. (21) becomes the noncommutative polynomial recurrence relation ($NCPRR$)

$$p_{N,n}^{(i)}+\zeta_i p_{N,n-1}^{(i)}+\eta_i p_{n-2}^{N,(i)}=0$$

$$\text{for } n\geqslant 1 \quad \text{and} \quad i=1,2. \tag{23}$$

Here $\zeta_1=-(\beta^{-1}\alpha\beta+\delta)$, $\eta_1=(\delta\beta^{-1}\alpha\beta-\gamma\beta)$, $\zeta_2=-(\gamma^{-1}\delta\gamma+\alpha)$, and $\eta_2=(\alpha\gamma^{-1}\delta\gamma-\beta\gamma)$ are the matrix coefficients. It is easy to see that the initial conditions are $p_{N,-1}^{(i)}=0$ and $p_{N,0}^{(i)}=I_N$. Notice that in the one-channel case, ζ and η become $\alpha+\delta=\mathrm{Tr}\,M$ and $\delta\alpha-\gamma\beta=\det M$, respectively. Thus, for *one-dimensional* systems the NCPRR is the Chebyshev polynomial recurrence relation and, at the same time, becomes the characteristic polynomial of the 2×2 transfer matrix. In the multichannel case, Eq. (23) contains noncommutative factors.

By solving the matrix recurrence relation it is possible to extend the transport analysis to a multichannel description. As was shown in Ref. 21 and will be outlined in Sec. IV and Appendix E, the matrix recurrence relations can be solved almost straightforwardly. Before continuing with this outline, let us assume that the polynomials $p_{N,m}$ are known and hence proceed to derive the superlattice scattering amplitudes and relevant physical quantities.

From the mathematical point of view, the generalized recurrence relations have some special implications which go beyond the purpose of this paper and will be discussed elsewhere in connection with the matrix representation of generalized orthogonal polynomials and noncommutative algebras, similar to those discussed recently by Gelfand *et al.*[31]

III. GENERAL FORMULAS FOR PHYSICAL QUANTITIES IN MULTICHANNEL PERIODIC SYSTEMS

Even though we do not yet know what the polynomials p_n are, we assume their existence and deduce general expression for the scattering amplitudes, the energy eigenvalues, the eigenfunctions, and some other transport properties in terms of the polynomials. Using Eqs. (20)–(22), it is easy to obtain

$$\alpha_{N,n}=p_{N,n}-\gamma^{-1}\delta\gamma p_{N,n-1}, \tag{24}$$

which together with Eq. (18) permits us to write the global multichannel transmission and reflection amplitudes as

$$t_{N,n}=[p_{N,n}-p_{N,n-1}(\gamma^{-1}\delta\gamma)^{\dagger}]^{-1}, \tag{25}$$

$$r_{N,n}=-[p_{N,n}-(\beta^{-1}\alpha\beta)p_{N,n-1}]^{-1}\gamma p_{N,n-1}. \tag{26}$$

These interesting results show that the n-cell scattering amplitudes can be expressed entirely in terms of single-cell transfer-matrix blocks (or single-cell transmission and reflection amplitudes r, t, r', and t') and the polynomials $p_{N,n}$. For time-reversal-invariant and spin-independent systems, $t_{N,n}$ is just the transpose of $t'_{N,n}$, and $\gamma=\beta^*$, $\delta=\alpha^*$. For spin-dependent systems $t'=k^T t^T k$ and $\gamma=k^T\beta^* k$, $\delta=k^T\alpha^* k$. The previous relations are simple and of general validity at the same time. In the particular, but very much used 1D one-channel case, the transmission amplitude

$$t_n=\frac{t^{\dagger}}{p_n t^{\dagger}-p_{n-1}} \tag{27}$$

takes the form

$$t_n=\frac{t^*}{t^* U_n-U_{n-1}}, \tag{28}$$

which is an extremely simple function of the Chebyshev polynomials of the second kind, $U_n(\alpha_R)$ and $U_{n-1}(\alpha_R)$ (evaluated *at* the real part of α), and of the single-cell transmission amplitude t. Using the identity $U_n U_{n-2}=U_{n-1}^2-1$, it is easy to show that the transmission coefficient $T_n=|t_n|^2$ can be written as[32]

$$T_n=\frac{T}{T-U_{n-1}^2(1-T)}, \tag{29}$$

with an evident resonant behavior. Here $T=|t|^2$ is the single-cell transmission coefficient. The transmission resonances occur precisely when the polynomial U_{n-1} becomes zero. Therefore the νth resonant energy $E_{\mu,\nu}$ is the solution of

$$(\alpha_R)_{\nu}=\cos\frac{\nu\pi}{n}, \tag{30}$$

with $\nu=1,2,3,\ldots,n-1$. The index μ labels the bands, as discussed above, and ν labels the intraband states. *These fundamental quantities cannot be determined with the current solid state theory but they can be with the present approach*. Although it is not clear that the actual experimental precision may allow one to discriminate the intraband energy states, we expect that for bounded finite periodic systems it will be possible to observe the fine energy structure using optical excitation experiments. This could have interesting consequences in the applied physics field. In Sec. V we will discuss some simple examples. Notice that, according to Eq. (29), each energy band contains, as often stated without proof in the textbooks, the same number of resonant energies as the number of confining wells.

Before going ahead and presenting new expressions for other physical quantities, let us apply the previous equations (29) and (30) to the sequence of square-barrier potentials formed in the conduction band of the superlattice $(\mathrm{GaAs/AlGaAs})^n$ shown in Fig. 1. For reasons of simplicity let us consider the 1D one-channel approximation. In Fig. 7, we present a series of graphs of the transmission coefficient T_n as a function of the particle's energy E and the number of cells n. It is evident that by increasing n, the band structure gradually builds up. The aim of the sequence of graphs in Fig. 7 is to illustrate the formation of the band structure as the finite periodic system grows, for fixed single-cell length $l_c=a_0+b_0$. One can observe the resonance splitting process. We can also observe that for n of order 5 the band structure at low energies is reasonably well defined.

Especially simple, in its functional structure, are the global Landauer multichannel resistance amplitudes $R'_{N,n}=r'_{N,n}(t_{N,n})^{-1}$ and $R_{N,n}=-(t'_{N,n})^{-1}r_{N,n}$. These quantities, in terms of the polynomials $p_{N,n}$, are just

$$R'_{N,n}=R'_{N,1}p_{N,n-1}, \quad R_{N,n}=R_{N,1}p_{N,n-1}.$$

Here, the tunneling and interference phenomena appear nicely factorized.

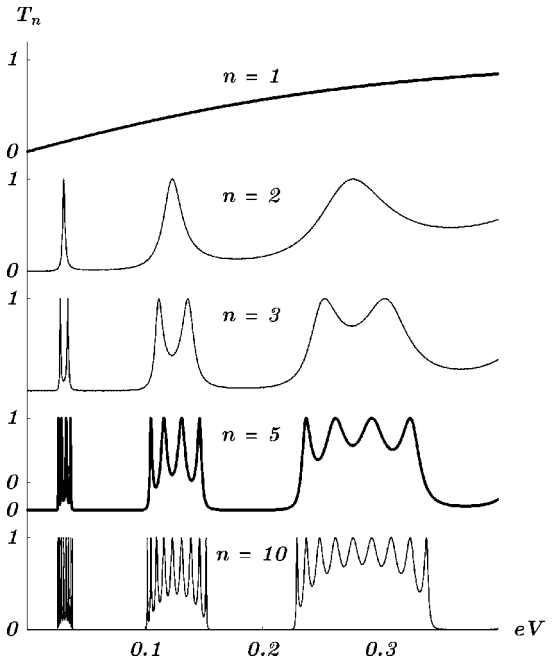

FIG. 7. The metamorphosis of the transmission coefficient T_n as a function of the particle's energy E and the number of cells n. The band structure is built up as the number of cells, n increases. The formation of bands is accompanied by a resonance splitting process. Notice that for n of the order of 5 the band structure at low energies is reasonably well defined.

A quantity often used in the transport theory is the Landauer multichannel conductance matrix $G_N = t_N (r_N^\dagger r_N)^{-1} t_N^\dagger$ which for the n-cell system becomes

$$G_{N,n} = \frac{1}{p_{N,n-1}} G_{N,1} \left(\frac{1}{p_{N,n-1}} \right)^\dagger . \tag{31}$$

In the one-channel case, the n-cell conductance is just

$$G_n = \frac{1}{(U_{n-1})^2} G. \tag{32}$$

The zeros of the polynomial determine both the points of divergence of G_n and the zeros of the resistance R_n. They also determine the resonant energy eigenvalues $E_{\mu,\nu}$ as well as the resonances of the global transmission coefficient T_n.

So far, we have given a number of nontrivial but extremely appealing relations. *The n-cell Landauer resistance amplitude is just the product of the one-cell Landauer resistance amplitude R and the polynomial* p_{n-1}. The polynomial $p_{N,n}$ has the information on the number of layers, n; on the number of channels, N; and, more importantly, on the complex but precise interference phenomena.

Another significant physical quantity to describe periodic systems is the superlattice wave function. In the standard theory of infinite periodic systems the Bloch's function is taken, with no further reflection, as *the* natural and obvious wave function. However, this is not quite correct for finite systems; the illusion of having a wave function with the apparent simplicity of Bloch's structure may considerably

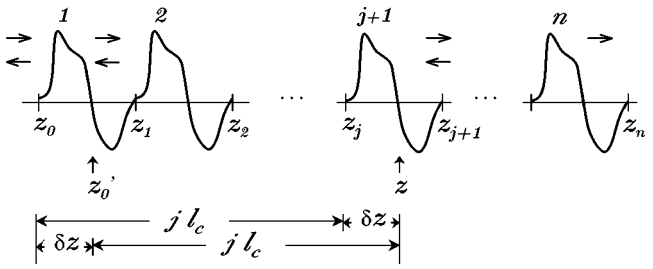

FIG. 8. The wave function at any point z in the $j+1$ cell (with $j=0,1,2,\ldots,n-1$) of an arbitrary n-cell system can be determined using the transfer matrix $M(z_0',z_0)$ for any $z_0 \leqslant z_0' \leqslant z_1 = z_0 + l_c$ and the relations (44)–(47). Since the wave vector at z is related to the wave vector at z_0 by the transfer matrix $M(z,z_0)$, we can obtain this matrix either as $M(z_j,z_0)$ followed by $M(z,z_j)$ or as $M(z_0',z_0)$ followed by $M(z,z_0')$ as depicted in the lower part of this figure.

complicate the calculation of other physical quantities. In the transfer-matrix theory the wave functions of finite periodic systems can be obtained in a very simple way. From the definition of the transfer matrix, we known that once the single-cell problem has been solved [i.e., once the transfer matrix $M(z_0,z_0')$, for any $z_0 \leqslant z_0' \leqslant z_1 = z_0 + l_c$ has been determined] one is able to evaluate the wave function at any other point $z = z_0' + j l_c$ within the $j+1$ cell of the periodic system or superlattice (with $j=0,1,2,\ldots,n-1$; see Fig. 8). In fact, the state vectors at z_0' and z are related by

$$\begin{pmatrix} a_j \vec{\varphi}(z) \\ b_j \overleftarrow{\varphi}(z) \end{pmatrix} = \begin{pmatrix} \alpha_j & \beta_j \\ \gamma_j & \delta_j \end{pmatrix} \begin{pmatrix} a_0 \vec{\varphi}(z_0') \\ b_0 \overleftarrow{\varphi}(z_0') \end{pmatrix}, \tag{33}$$

with

$$\alpha_j = p_j - \gamma^{-1} \delta \gamma p_{j-1}, \tag{34}$$

$$\beta_j = \beta^{-1} p_{j-1}, \tag{35}$$

$$\delta_j = p_j - \beta^{-1} \alpha \beta p_{j-1}, \tag{36}$$

$$\gamma_j = \gamma^{-1} p_{j-1}. \tag{37}$$

In the same way, the state vector at z is related with the state vector at the end of the superlattice, where only the transmitted component must be considered.

For an open system, as the one shown in Fig. 8, the right-side propagating state vector at z is

$$\vec{\varphi}(z) = \vec{\varphi}(z_0') \left(\alpha_j - \beta_j \frac{\gamma^{-1} p_{n-1}}{(p_n - \beta^{-1} \alpha \beta p_{n-1})} \right), \tag{38}$$

and the left-side propagating state vector at z is

$$\overleftarrow{\varphi}(z) = \vec{\varphi}(z_0') \left(\gamma_j - \delta_j \frac{\gamma^{-1} p_{n-1}}{(p_n - \beta^{-1} \alpha \beta p_{n-1})} \right). \tag{39}$$

Evaluating these state vectors at $E_{\mu,\nu}$, we have the corresponding resonant states. In the 1D one-channel case the matrix elements $\alpha_j, \beta_j, \ldots$ are simple functions of the Chebyshev polynomials, as can be inferred from Eqs. (21) and (34)–(37). These matrix elements, together with Eqs.

(38) and (39), give the wave functions. In Sec. V, the wave functions and resonant functions for a particular example will be evaluated and plotted. These and the other relations already presented in this section are some of the general expressions obtained in this theory. In the subsequent parts we will extend this approach to describe the physics of bounded and quasibounded systems and real semiconductors.

As mentioned in the Introduction, a significant characteristic of the global or superlattice physical quantities resides in their functional structure, expressed entirely in terms of the corresponding single-cell quantities and the polynomials $p_{N,m}$. It is clear then that in order to evaluate these quantities we first need to determine the polynomials $p_{N,m}$. This will be done in the next section. Keep in mind that in the 1D case we already found that $p_{1,m}$ is precisely a Chebyshev polynomial of the second kind, U_m.

IV. POLYNOMIALS $P_{N,n}$

We shall now briefly refer to the solutions of the recurrence relations. In the 1D one-channel case, α, β, γ, and δ are complex numbers, and the recurrence relations for β_n (or δ_n) and p_n reduce to the Chebyshev's recurrence relation

$$p_n + g_1 p_{n-1} + p_{n-2} = 0, \tag{40}$$

with $p_{-1}=0$, $p_0=1$, and

$$g_1 = -\operatorname{Tr} M. \tag{41}$$

Although the Chebyshev polynomials and the generating functions method are well known, we shall recall them in Appendix E 1 to show the notation employed and to introduce the procedure used in the most general case. Using the eigenvalue representation, i.e., the eigenvalues λ_1 and λ_2 of the 2×2 transfer matrix, the Chebyshev polynomial of the second kind can be written as

$$p_n = \frac{\lambda_1^{n+1} - \lambda_2^{n+1}}{\lambda_2 - \lambda_1}. \tag{42}$$

In Bargmann's representation, the unit-cell amplitudes t, r and the eigenvalues λ_1, λ_2 for a time-reversal-invariant system can be written, respectively, as

$$t = e^{i(\phi_u - \phi_v)} \frac{1}{\cosh \chi}, \tag{43}$$

$$r = e^{-2i\phi_u} \tanh \chi, \tag{44}$$

$$\lambda_{1,2} = \cos(\phi_u - \phi_v)\cosh \chi \pm \sqrt{[\cos(\phi_u - \phi_v)\cosh \chi]^2 - 1}. \tag{45}$$

For $N \geqslant 2$, we have the MRR

$$p_{N,n} = -\zeta p_{N,n-1} - \eta p_{N,n-2}, \tag{46}$$

with $\zeta = -(\beta^{-1}\alpha\beta + \delta)$ and $\eta = (\delta\beta^{-1}\alpha\beta - \gamma\beta)$. This is an interesting and important problem. Solving this relation, we can expect a multichannel description of the transport processes in finite periodic systems. Even though the problem might seem rather complicated, it is nevertheless soluble.[4,21] We show, in Appendix E 2, that the matrix polynomials satisfying the matrix recurrence relation are

$$p_{N,n} = \sum_{k=0}^{n} \sum_{l=0}^{k} p_{N,l} g_{k-l} q_{n-k} \quad \text{for} \quad n < 2N \tag{47}$$

and

$$p_{N,n} = \sum_{k=0}^{2N-1} \sum_{l=0}^{k} p_{N,l} g_{k-l} q_{n-k} \quad \text{for} \quad n \geqslant 2N. \tag{48}$$

Here the coefficients g_j, q_n are the symmetric functions

$$g_j = (-)^j \sum_{l_1 < l_2 < \cdots < l_j}^{2N} \lambda_{l_1}\lambda_{l_2}\cdots\lambda_{l_j}, \quad g_0 = 1, \tag{49}$$

and

$$q_n = \sum_{i=1}^{2N} \frac{\lambda_i^{2N+n-1}}{\prod_{j\neq i}^{2N} (\lambda_i - \lambda_j)} I_N. \tag{50}$$

It is obvious from these results that, in order to obtain a polynomial $p_{N,n}$, one has to first determine the initial $2N-1$ polynomials $p_{N,l}$, which can be obtained by using the matrix recurrence relation. Notice also that for a given number of channels, $N \leqslant n/2$, we have to evaluate the sum

$$p_{N,n} = \sum_{k=0}^{2N-1} c_{k,n} p_{N,k},$$

$$\text{with} \quad c_{k,n} = q_{n-k} \sum_{l=0}^{k} g_{k-l}, \tag{51}$$

where the scalars $c_{k,n}$ are the only quantities which depend on the size of the system $L = n l_c$.

Based on these results we now consider some simple realizations, which when applied to multichannel transmission coefficients define some useful relations and the *transition probabilities*.

A. One propagating mode

For $N=1$ and n cells, Eq. (47) reduces to

$$p_{1,n} = c_{0,n} - c_{1,n} g_1 = q_{1,n} = q_n = \sum_{i=1}^{2} \frac{\lambda_i^{n+1}}{\prod_{j\neq i}^{2} (\lambda_i - \lambda_j)}, \tag{52}$$

which is precisely the well-known Chebyshev polynomial $U_n(\mathrm{tr}M/2)$ of the second kind given in Eq. (42).

B. Two propagating modes

For $N=2$ and $n \geqslant 4$, the 2×2 matrix polynomials $p_{2,n}$ are determined from

$$p_{2,n} = c_{0,n} I_2 - c_{1,n}\zeta + c_{2,n}(\zeta^2 - \eta) - c_{3,n}(\zeta^3 - \zeta\eta - \eta\zeta), \tag{53}$$

with ζ and η the coefficients of the matrix recurrence relation. Once the matrices ζ, $\zeta^2-\eta$, and $\zeta^3-\zeta\eta-\eta\zeta$ are calculated, all we need is to evaluate the coefficients $c_{k,n}$ for the corresponding number of cells n. For systems with two propagating modes, the matrices $p_{2,n}$ play the same role as the Chebyshev polynomials in the case of one propagating mode. The matrix polynomials are, however, more complex and contain abundant information on the rather complicated multichannel transport processes.

C. Transition probabilities and channel mixing

The transmission amplitude matrices in Eqs. (25) and (26) depending on the polynomials $p_{N,n}$ are loaded with information and open up the possibility of calculating quantities such as channel *transition* probabilities, whose amplitudes are given by the transmission matrix elements $t_{n,ij}\equiv(t_n)_{ij}$ for $i\neq j$. In principle, these quantities provide information on the channel mixing phenomena. An incoming particle in the jth propagating mode might come out from the scatterer system in the ith propagating mode. These types of processes are induced by channel coupling interactions, expected whenever the channel coupling parameters K_{ij}, for $i\neq j$, are different from zero. The transmission probability $T_{Nn,ij}$ (or just $T_{n,ij}$), from channel j on the left-to channel i on the right-hand side, is obtained from

$$T_{n,ij}=|t_{Nn,ij}|^2=|\{[p_{Nn}-p_{Nn-1}(\beta^{-1}\alpha\beta)^T]^{-1}\}_{ij}|^2. \tag{54}$$

Being able to calculate these transmission probabilities, it is possible to evaluate other quantities as interesting as the total transmission probability $T_{Nn,i}$ (or just $T_{n,i}$) to channel i, which regardless of the incoming channel j is given by

$$T_{n,i}=\sum_{j=1}^{N}|t_{Nn,ij}|^2. \tag{55}$$

A quantity where the channel information disappears, and is certainly much easier to measure, is the well-known conductance or total transmission probability T_n through the n-cell system. This is defined as

$$G_n=T_n=\mathrm{Tr}\,t_{Nn}t_{Nn}^{\dagger}=\sum_{i=1}^{N}T_{n,i}=\sum_{i,j=1}^{N}|t_{Nn,ij}|^2. \tag{56}$$

We are now ready to calculate all these quantities and discuss the behavior of the transmission-reflection probabilities and other interesting superlattice properties for both arbitrary and specific potential functions.

V. ILLUSTRATIVE FINITE PERIODIC SYSTEMS

In the first part of this section we will apply our approach to several examples of one-channel periodic systems and in the second part to simple periodic systems of two and three propagating modes.

A. One-channel systems

For the purpose of discussing general qualitative properties, with no reference to any particular potential function, we will first look into the transmission coefficients in a 1D system as functions of the Bargmann parameters χ and ϕ. We will then use the general results of Sec. III to evaluate transport properties for specific 1-D systems. The physical properties of interest that will be considered here include the band structure building process mentioned above, the band structure tailoring, the resonant energies and wave functions, the level density, and the Kronig-Penney model. In the last part of this subsection, we shall also consider an optical multilayer system.

1. Band structure as a general property of periodic systems

In general we think of transfer matrices as associated with some specific system. It is possible, however, to think of transfer matrices expressed in terms of nonspecific and rather general parameters, such as the Bargmann parameters mentioned before. Using these parameters we can analyze the behavior of some functions appearing in the universal expressions obtained so far and deduce universal properties related to any periodic systems. For this purpose it is convenient to plot the physical quantities as functions of the free parameters. The most general 1D (one-channel) transfer matrix of the orthogonal class contains three free parameters,[24] only two of them being relevant to the physical quantities considered here. In Bargmann's representation we have

$$t=e^{i(\phi_u-\phi_v)}\frac{1}{\cosh\chi}\equiv e^{i\phi}\frac{1}{\cosh\chi}, \tag{57}$$

$$g_1=\cos(\phi_u-\phi_v)\cosh\chi\equiv\cos\phi\cosh\chi, \tag{58}$$

and

$$\lambda_{1,2}=\cos\phi\cosh\chi\pm\sqrt{(\cos\phi\cosh\chi)^2-1}. \tag{59}$$

The *single-cell* Landauer conductance $G=\sinh^{-2}\chi$ and the *single-cell* transmission probability $T=\cosh^{-2}\chi$ do not depend on the phase ϕ; hence, they are monotonic functions of χ as can be seen in Fig. 9(a). For χ varying from 0 to infinity, T decreases monotonously from 1 to 0, while G goes from infinity to zero. If we plot these quantities as functions of the energy [see Fig. 10(a) below], they will increase as the energy grows since χ decreases with the energy.

The n-cell conductance $G_n=G/(p_{n-1})^2$ and the n -cell transmission coefficient $T_n=T/[T-p_{n-1}^2(1-T)]$ depend on the phase ϕ through the polynomials p_{n-1}, which, as mentioned before, carry information on the periodic nature of the system and on the phase interference phenomena. The appearance of a resonant band structure [see Fig. 9(b)] is a universal effect independent of the specific potential shape. The band and gap widths are given by $\mathrm{Tr}\,M/2$. In order to understand the role of the polynomial p_n, we plot the nine-cell transmission probability T_9 together with the Chebyshev polynomial p_{9-1}, for a fixed χ in Fig. 9(b). The Chebyshev polynomial p_{n-1}, evaluated at $\alpha_R=\mathrm{Tr}\,M/2$, determines not only the position and bandwidths, it determines also the po-

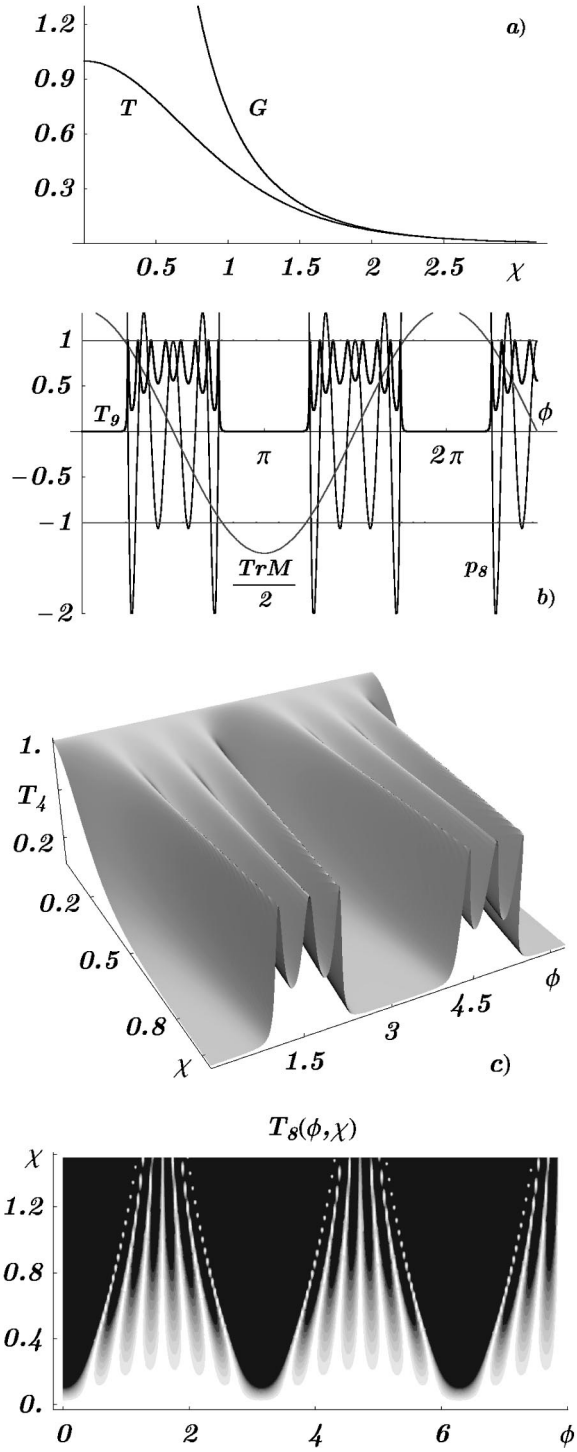

FIG. 9. Various physical quantities plotted as functions of the Bargmann parameters. (a) The single-cell Landauer conductance $G=\sinh^{-2}\chi$ and the single-cell transmission probability $T=\cosh^{-2}\chi$ are monotonous functions of χ. (b) The nine-cell transmission coefficient T_9 together with the Chebyshev polynomial p_{9-1} and the transfer matrix trace $\mathrm{Tr}\,M/2$, are plotted as functions of the phase ϕ for a fixed χ. From these figures and the bahavior of the transmission coefficients in (c), it is evident that the responsible of the band structure and the resonant behavior is the phase coherence phenomena.

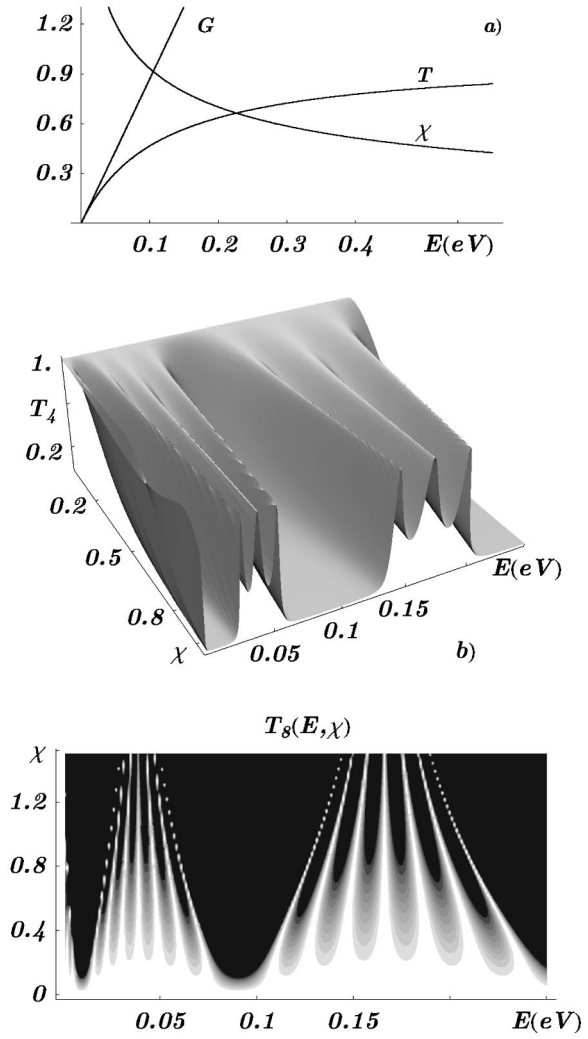

FIG. 10. The transmission coefficients for a periodic system of δ-barrier potentials, separated consecutively by a distance a_0, plotted as functions of the Bargmann parameter χ and the incoming particle's energy E. The bandwidths increase with the energy, as corresponds to the monotonous grow of the phase ϕ with the energy (see Fig. 5).

sition of the tunneling resonances. Remember that α_n satisfies recurrence relations similar to those of p_{n-1}. This fact is especially interesting in relation to multichannel systems. To conclude this part we plot in Fig. 9(c) the global four-cell transmission coefficient $T_4(\phi,\chi)$ and the contour graph for $T_8(\phi,\chi)$ (here the black regions correspond to lower transmission coefficients), both as functions of ϕ and χ. In these figures the previously discussed behavior is evident: varying ϕ we generate the resonant structure while varying χ the gap and the allowed energy bands are distinguished very clearly. In terms of the free parameters ϕ and χ, the band structure appears as a periodic repetition of the single-band behavior, i.e., $T_n(\phi,\chi)=T_n(\phi+2\pi,\chi)$. If, instead, we plot these quantities as functions of the energy and the potential parameters, the bandwidths will be different at different energy regions (see Fig. 10 below).

2. Transmission through square- and δ-barrier potential superlattices

Let us now consider two specific and well known 1D potential functions: the *square-* and *δ-barrier* potentials. For δ barriers of strength V_0, separated consecutively by a distance a_0, the Bargmann parameters χ and ϕ are

$$\chi = \cosh^{-1}\left(1+\frac{V_0}{2E}\right)^{1/2} \tag{60}$$

and

$$\phi = \frac{\sqrt{2m_eE}}{\hbar}a_0 - \tan^{-1}\sqrt{\frac{V_0}{2E}}. \tag{61}$$

Using these parameters, we can easily evaluate the transmission coefficients shown in Fig. 10. Their remarkable qualitative similarity with the corresponding coefficients for the arbitrary and nonspecific periodic system in Fig. 9 is evident. The transmission coefficients are now plotted as functions of the energy E and the parameter χ (which also depends on the energy). As suggested before and can be seen in Fig. 10(a), the parameter χ is a monotonous decreasing function of the energy, while T and G increase.

For square barriers with height V_0 and width b_0 separated by potential wells of thickness a_0, the Bargmann parameters χ and $\phi \equiv \phi_u - \phi_v$ are (see Appendix B)

$$\chi = \cosh^{-1}\left[1+\frac{v_0^2}{\epsilon(\epsilon-v_0)}\sinh^2\left(\frac{\sqrt{2m_b^*(\epsilon-v_0)}}{\hbar}\right)^{1/2}\right] \tag{62}$$

and

$$\phi = \frac{\sqrt{2m_v^*\epsilon}}{\hbar}\left(1+\frac{a_0}{b_0}\right) + \tan^{-1}\left[\frac{2\epsilon-v_0}{\sqrt{\epsilon(\epsilon-v_0)}}\tanh\left(\frac{\sqrt{2m_b^*(\epsilon-v_0)}}{\hbar}\right)\right]. \tag{63}$$

Here, m_v^* and m_b^* are the effective masses in the valley and barrier, respectively,[33] $\epsilon = Eb_0^2$ and $v_0 = V_0 b_0^2$. As mentioned before, it is not necessary to use the Bargmann's representation, unless one feels it convenient or one is interested in analyzing generic properties as has been done in the previous subsection. Using these functions and the superlattice formulas given above, we can explore physical properties such as the band structure, the resonant energies, the resonant superlattice functions, the density of states, the superlattice tunneling time, the peak to valley ratios, etc.

In Fig. 11, the same quantities as in Figs. 9 and 10 but now for square-barrier chains are plotted. The qualitative similarities are also evident. The formation of resonant bands with higher transmission probabilities at certain energies is definitely a phase coherence effect. At low energies the vanishing of the transmission probability in the gap regions is a consequence of the phase interference phenomena and the tunneling effect. This band effect becomes much more pronounced as the number of cells, n, increases. At this point it

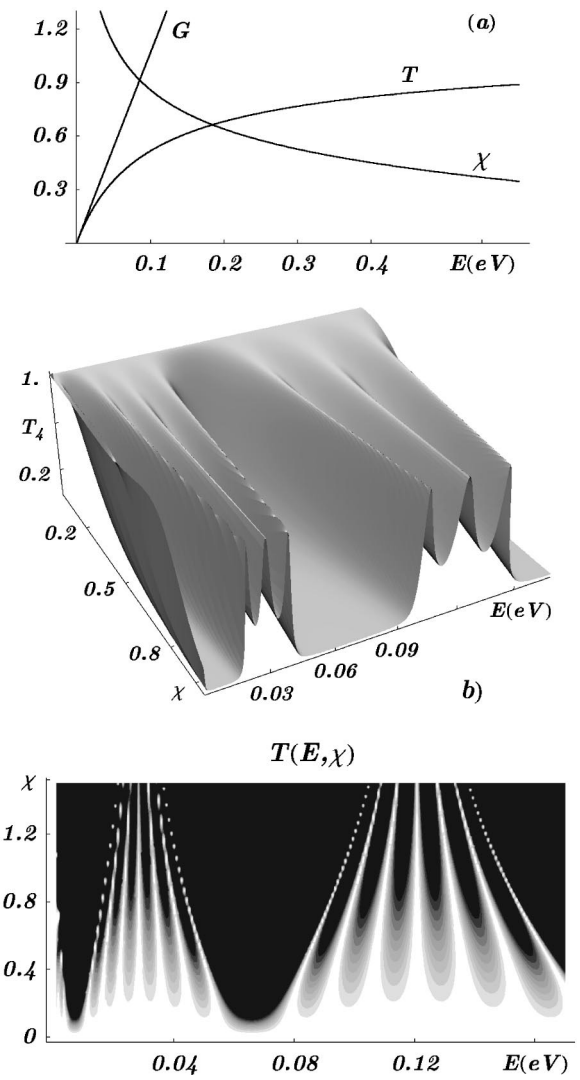

FIG. 11. The transmission coefficients for a periodic system of square barriers with height V_0 and width b_0, separated by potential wells of width a_0, are plotted as functions of the Bargmann parameter χ and the incoming particle's energy E. The behavior is qualitatively similar as for the δ-barrier potential and as for the arbitrary and generic case plotted in Fig. 8.

is worth emphasizing that the periodicity and finiteness are fully incorporated in the theory through simple and precise functional dependence of the physical quantities upon the polynomials p_n. It is also worth emphasizing that all we need in order to evaluate an important number of relevant superlattice physical quantities is to determine, with the highest possible precision, the single-cell transfer matrix. As mentioned before, the band structure in the one-mode approximation is easily obtained by plotting the transfer-matrix trace

$$Tr\, M_0 = 2\cos\phi\cosh\chi.$$

Other quantities will be considered in the next subsection.

3. Resonant energies and resonant wave functions, level density, and the KP model

Here we will present some specific results for the resonant energies and resonant states in the transport process through

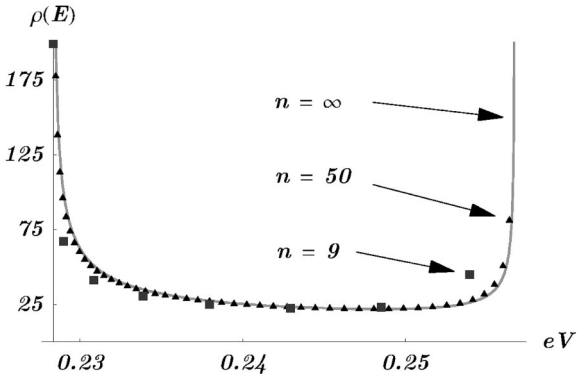

FIG. 12. The level density in the first subband of a finite and an infinite (Kronig-Penney) GaAs $(Al_{0.3}Ga_{0.7}As/GaAs)^n$ superlattice with $a=100$ nm, $b=30$ nm, and $V_0=0.23$ eV. The discrete energy spectrum plotted for $n=9$ and $n=50$ approaches the continuous spectrum of the Kronig-Penney model when $n\to\infty$.

an open square-barrier superlattice, as the one shown in Fig. 3. Eigenvalues and eigenfunctions will be discussed in the sequel (part II) of this theory. As mentioned above, the νth resonant energy $E_{\mu,\nu}$ is obtained by solving the implicit equation

$$(\alpha_R)_\nu = \cos\frac{\nu\pi}{n},$$

$$\text{with} \quad \nu = 1,2,\ldots,n-1,$$

where α_R is the real part of α and $(\alpha_R)_\nu$ is the νth zero of the Chebyshev polynomial. The index μ labels the bands, and the index ν labels the intraband energy resonances, peculiar to periodic systems and entirely determined by phase coherence. In the transfer-matrix approach the allowed energy bands are those energies which satisfy the condition $\cos\phi\cosh\chi = |\alpha_R| \leqslant 1$. For the n-cell square-barrier system, whose transfer matrix is calculated in the Appendix A, the resonant energy equation becomes

$$\cos k_\nu a_0 \cosh q_\nu b_0 - \frac{k_\nu^2 - q_\nu^2}{2k_\nu q_\nu}\sin k_\nu a_0 \sinh q_\nu b_0 = \cos\frac{\nu\pi}{n}, \tag{64}$$

with $k_\nu^2 = 2m_v^* E_{\mu,\nu}/\hbar^2$ and $q_\nu^2 = 2m_b^*(V_0 - E_{\mu,\nu})/\hbar^2$. Each of the energy bands contains the same number of resonant energies as the number of confining wells, in this case $n-1$. In Fig. 12, some of these energies and the associated level densities are plotted for different values of n. Notice that the level density behavior as a function of n tends rapidly to that of the Kronig-Penney model,[34] although the continuous spectrum limit is only reached when $n\to\infty$.

For TRI scattering systems like the one shown in Fig. 8, the wave function at z is given by

$$\Psi(z,E) = \vec{\varphi}(z_0')\left[\alpha_j + \beta_j^* - (\alpha_j^* + \beta_j)\frac{\beta_n^*}{\alpha_n^*}\right],$$

$$\text{with} \quad j = 0,1,\ldots,n-1. \tag{65}$$

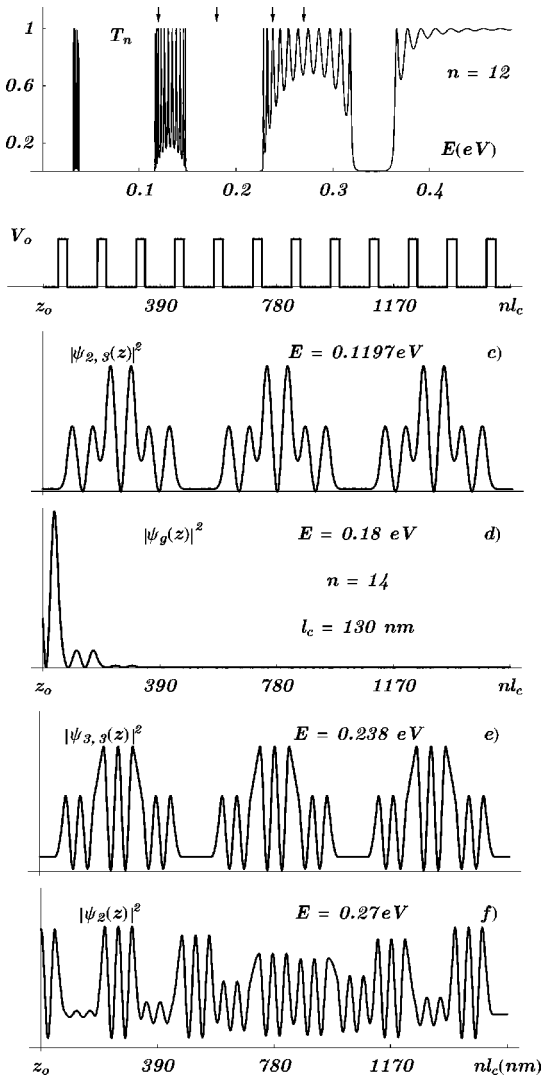

FIG. 13. Extended, localized, and resonant wave functions for independent electrons moving along a superlatice like the one shown here and for the energy values indicated with an arrow in the transmission coefficient. In (c) and (e) we have the resonant wave functions $\phi_{\mu,\nu}$ obtained by evaluating Eq. (75) at resonant energies $E_{\mu,\nu}$ in the second and third subbands, obtained from Eq. (74). The number of oscilation of the envelope corresponds to the index ν. In (d) we have a localized wave function obtained by evaluating Eq. (75) for an energy in the gap. In (f) the wave function is evaluated at an arbitrary energy in the third allowed energy band.

It is important to notice that the wave function depends on the various potential parameters, the particle's energy E, and the total number of cells, n. Notice also that while $0 \leqslant z_0' \leqslant l_c$, the coordinate z can take values between 0 and nl_c. When z is in the first cell it coincides with z_0', so that $\Psi(z_0,E) = \vec{\varphi}(z_0)(1-\beta_n^*/\alpha_n^*)$, since for $j=0$, $\alpha_0=1$ and $\beta_0=0$. It is evident that evaluating the function $\Psi(z,E)$ at the resonant energies $E_{\mu,\nu}$ we get the corresponding resonant function

$$\Psi_{\mu,\nu}(z) = \Psi(z,E_{\mu,\nu}). \tag{66}$$

In Figs. 13(c)–13(f) we plot the wave function along the superlattice GaAs(AlGaAs/GaAs) (Ref. 12) at four different

energies indicated with arrows in the transmission coefficients in Fig. 13(a). While in Figs. 13(c) and 13(e), the functions $|\Psi_{\mu,\nu}(z)|^2$ correspond to the third resonant energies in the second ($\nu=2$) and third ($\nu=3$) energy bands (in these cases the resonant bound-state functions are modulated by an oscillating envelope function with $\nu+1$ minima), in Fig. 13(d) the wave function is evaluated for an energy in the gap between the second and third bands. In Fig. 13(f) the wave function is plotted for an arbitrary energy E ($\neq E_{\mu,\nu}$) inside a band. In the last case we have an extended wave function with a very complicated behavior along the superlattice. At $z=0$ and $z=nl_c$ the resonant wave functions are different from zero, because they describe not only the extended but also the transmitted states, unless the energy lies in a gap region and the probability of finding the particles at the ends of the system is different from zero. This will, of course, change for bounded systems. The same happens with the function $|\Psi_2|^2$ in Fig. 12(f), where $\mu=2$. In Fig. 13(d), the behavior of the wave function in the gap is not only compatible with the well-known vanishing of the transmission coefficient, it shows also a localization effect induced by the phase coherence, which is an appealing result.

4. Band structure tailoring: Levels and bands in the gaps

One of the most significant and interesting properties of periodic systems, in general, and of multilayer superlattices, in particular, is the possibility of tailoring their band structure. Pronounced macroscopic effects, such as the increase of the electric conductivity of real semiconductors (containing defects and different types of impurity atoms), rest on the appearance of extra energy levels in the gaps of ideal semiconductors. The superlattices become in this sense quite attractive because of the possibility of modifying their periodicity by ''inserting'' at will extra energy levels in the subband gaps. Different types of topological defects, referred to here for the sake of simplicity as ''impurities,'' can effectively be created in these heterostructures by changing the valley (barrier), depth (height), or width of certain layers. As a consequence, the band structure is modified and the resonant peaks move to new positions. Using the method and formulas presented here, it is rather simple to determine these kind of effects on the band structure and, especially, on the impurity-level position in the band gaps. To illustrate this, we shall consider *one* and *two* substitutional ''valley impurities'' (with valley widths a_{0i}) immersed in an otherwise periodic square-barrier or δ-barrier chain. In our examples, the valley impurities are produced by varying the well's width such that the impurity width is $a_{0i}=z_i a_0$ with $z_i \neq 1$. We can also vary the valley depth. This implies a different *wave number* k_i at the impurity layer. Other changes of local-potential parameters are also possible.

In general, if we have s valley impurities in a chain of n cells, the whole superlattice transfer matrix will be given by

$$M_n = M_{n_1} W_{i_1} M_{n_2} \cdots M_{n_s} W_{i_s} M_{n_{s+1}},$$

$$\text{with} \quad n = \sum_{j=1}^{s+1} n_j, \tag{67}$$

and

$$W_i = \begin{pmatrix} e^{id_i k_i} & 0 \\ 0 & e^{-id_i k_i} \end{pmatrix} = \begin{pmatrix} w_i & 0 \\ 0 & w_i^* \end{pmatrix}, \tag{68}$$

as the valley-impurity transfer matrix. For a chain with a few impurities, α_n and β_n can easily be calculated using for each of the periodic sectors the already known expression

$$\alpha_{n_l} = p_{n_l} - p_{n_{l-1}}(\beta^{-1}\alpha\beta), \tag{69}$$

which in the one-channel limit is just

$$\alpha_{n_l} = p_{n_l} - p_{n_{l-1}}\alpha, \tag{70}$$

where p_{n_l} is the Chebyshev polynomial of order n_l evaluated at $\mathrm{Re}(\alpha)$. In the particular case of only *one* impurity located, say, at the center of the chain (which means $n_1=n_2$), we have

$$\alpha_n = \alpha_{n_1} w_i \alpha_{n_1} + \beta_{n_1} w_i \beta_{n_1}^* = -(t_n^\dagger)^{-1}. \tag{71}$$

In order to evaluate some physical quantities and to observe the impurity effects on a specific band structure, let us consider again a square-barrier superlattice like the one shown in Fig. 14(a) with $a_0=2$ nm, $b_0=10$ nm, and $V_0=0.23$ eV. For this system, having a valley impurity at the center of the superlattice and $n=10$ barriers, we plot in Figs. 14(b)–14(f) the total transmission coefficient for different values of the impurity width $a_{0i}=z_i a_0$. When $z_i<1$, the impurity valley width is narrower than a_0 and corresponds, qualitatively, to a negative difference $\Delta Z<0$ between the impurity and the host core charge numbers (acceptors of electrons). In the left-hand side column, the transmission coefficients are plotted for $z_i=0.9,0.8,\ldots,0.5$. As expected when $\Delta Z<0$, an energy level separates from the upper band edges and moves towards the upper bands as z_i departs from 1. It is interesting to notice that the resonances in the bands are strongly modified. When the energy level approaches the next upper band a new energy level separates from the opposite side of that band. This kind of *energy-level repulsion* and *band crossing* are interesting and novel effects that can clearly be seen in this example. For the energy level appearing between the second and third bands, the band-crossing effect occurs when $z_i \sim 0.5$. Similarly, for wider ($z_i>1$) impurity valleys the behavior corresponds to donors of electrons with $\Delta Z>0$. As z_i departs from 1 an energy level separates from the lower band edge and moves towards lower energies as z_i increases. It is obvious that by adjusting the parameter z_i we can place the impurity level at any desired position.

Increasing the number of impurities, but keeping constant their separation, a second-order superlattice is built up and the coherence phenomena manifests, producing another interesting impurity effect in the band structure. The single resonances in the gaps split and narrow bands appear, precisely where the single peaks were at before, with as many resonances as impurities contained in the superlattice. To illustrate this behavior, we consider the systems shown in

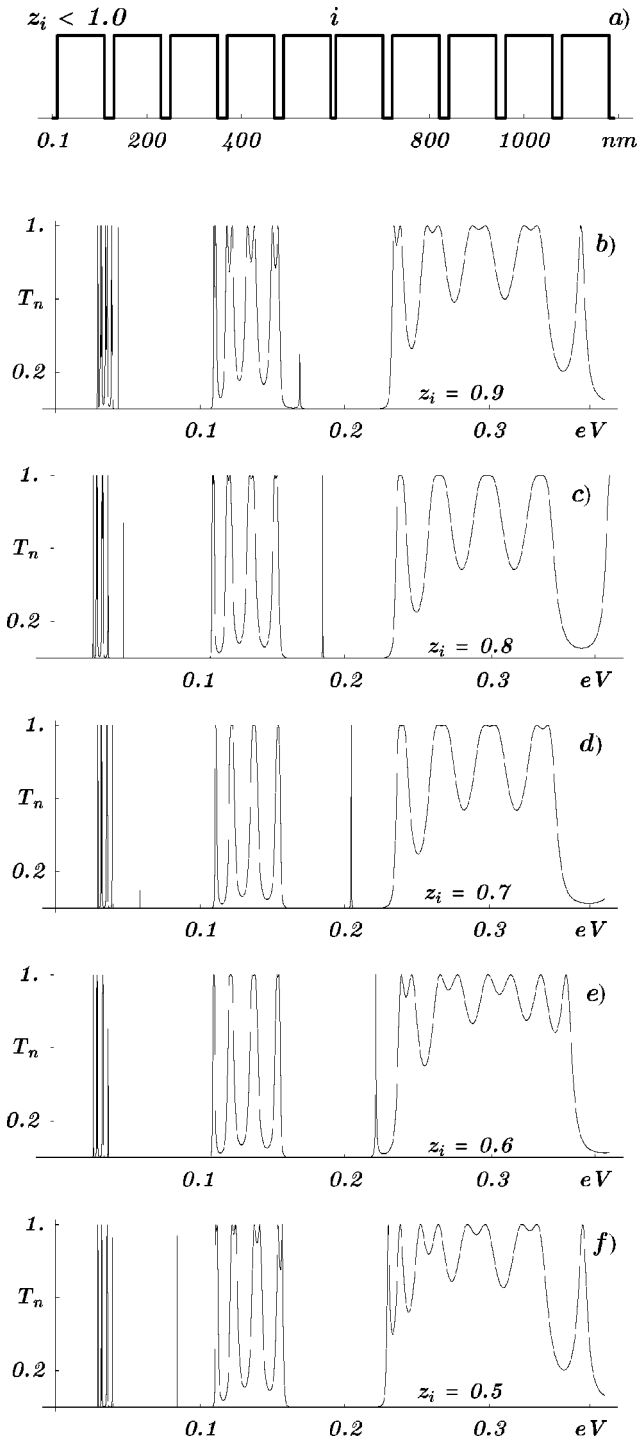

FIG. 14. In this sequence we have the transmission coefficients and the modified band structure for a periodic potential containing one impurity with valley width $a_0 = z_i a_0$ and $z_i < 1$ which corresponds, qualitatively, to a negative difference $\Delta Z < 0$ between the impurity and the host core charge numbers (acceptors of electrons). As z_i departs from 1, the *levels in the gap* move towards higher energies. The level repulsion effect is also apparent in these figures. For $z_i \sim 0.5$, the level in the gap enters into the band and another level abandons the band from the opposite band edge.

Figs. 15(a) and 15(b), with one- and two-valley impurities, respectively. In the left-hand side column the transmission coefficients are shown for the one-impurity system, while in the right-hand side column, the transmission coefficients corresponds to the system with two impurities. By adjusting the impurity valley width and enlarging the superlattice to increase the number of impurities, narrow bands can also be generated at any desired position. If, on the other hand, we keep the number of impurities constant while increasing the total number of cells, i.e., lowering the impurity concentration, the bands in the gaps remain in the same positions but their width diminishes rapidly. To study this effect, let us consider superlattices of different size ($n = 20$, 28, and 36) but with the same number $s = 3$ of (equidistant) impurities. In Fig. 16 we plot the transmission coefficients. Going down, from Fig. 16(a) to Fig. 16(c) the size n increases (while the impurity concentration diminishes), and simultaneously the impurity bands become narrower. It is interesting to notice that the principal bands are strongly modified and even break in thinner bands. The appearance of multiple, narrower, close minibands might favor the conduction process.

The effects on the band structure are qualitatively similar for square- and δ-barrier chains. Although these results are well known and can be calculated by evaluating products of transfer matrices, our formulas permit simpler and easy calculations. The technological consequences of playing with these properties may be of great interest. We presented here an easy method for making parametric changes and for evaluating the appearance of levels in the gaps and for band structure tailoring.

As for the one-impurity or defect chains, the number of resonant pairs of levels per unit energy depends on z_i.

5. Multilayer optical power limiting

Optical multilayer systems have been considered for studying optical properties. The superluminal tunneling times have been studied within this approach. The phase time predictions[22] agree impressively well with the experimental measurements.[35] Linear and nonlinear response system properties have been also of interest recently.[23] Linear response systems are described by

$$\frac{d^2\mathcal{E}}{dz^2} = -\epsilon_1 k_0^2 \mathcal{E} \tag{72}$$

and the nonlinear response systems, in the ''single-layer approximation'' of Ref. 23, by

$$\frac{d^2\mathcal{E}}{dz^2} = -\epsilon_2 k_0^2 (1 - |\mathcal{E}_0|^2)\mathcal{E}. \tag{73}$$

Here ϵ_i is the dielectric constant and $\mathcal{E}_0$ the incident electric field with frequency $\omega_0 = k_0 c$. It is easy to show that for a system of alternating layers of linear and nonlinear responses, with wave numbers $k = k_0\sqrt{\epsilon_1}$ and $K = k_0\sqrt{\epsilon_2(1 - |\mathcal{E}_0|^2)}$, and widths a_0 and b_0, respectively, the transfer-matrix elements are

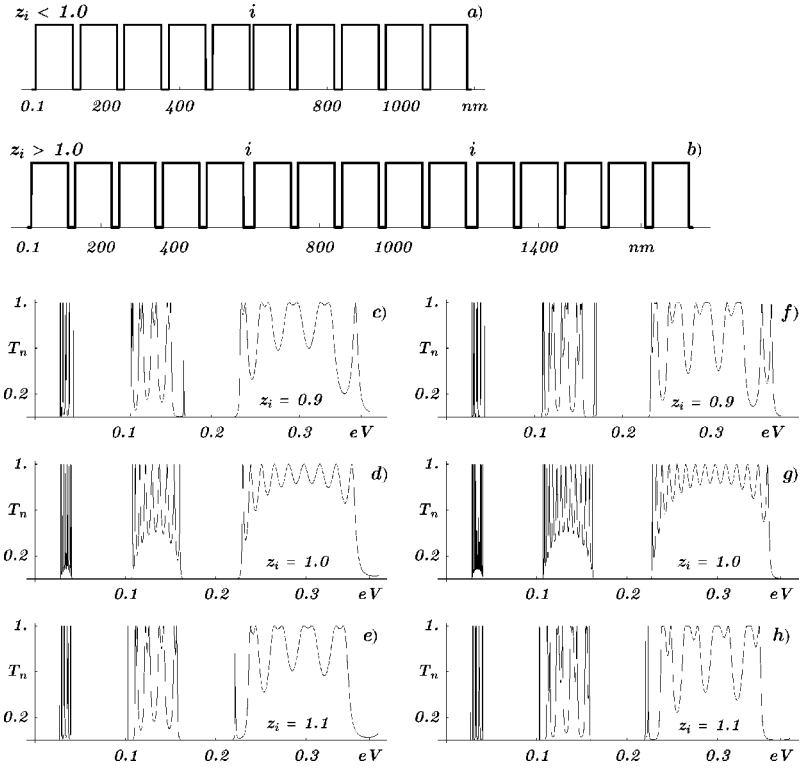

FIG. 15. The transmission coefficients in the left and right columns correspond to superlattices with one and two impurities, respectively. In each column we have $z_i=0.9$, 1.0, and 1.1. As expected for $z_i>1$, corresponding (qualitatively) to a positive difference $\Delta Z>0$ between the impurity and the host core charge numbers (donors of electrons), the level in the gap separates from the lower band edge. It is also nice to see that increasing the superlatice and simultaneously the number of impurities, with the same z_i, the single level in the gap splits to form a miniband in the gap.

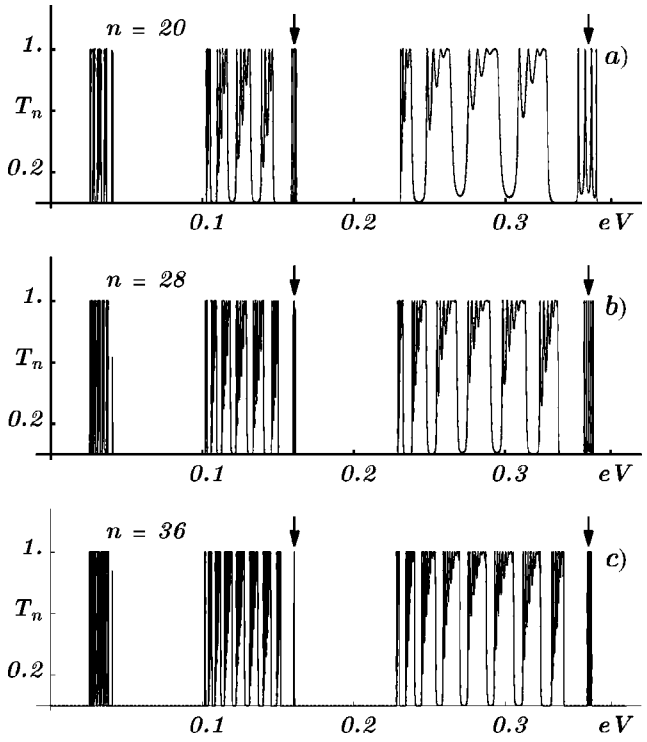

FIG. 16. The purpose of the three graphs here is to show the impurity concentration effect. Keeping the number of impurities constant ($n_i=3$) but increasing the total number of cells [from $n=20$ in (a) to $n=36$ in (c)], i.e., lowering the impurity concentration, the bands in the gaps remain in the same positions but their width reduce rapidly.

$$\alpha=\frac{1}{4kK}[(K+k)^2e^{i\theta_1}-(K-k)^2e^{-i\theta_2}] \tag{74}$$

and

$$\beta=\frac{(K^2-k^2)}{4kK}(e^{i\theta_2}-e^{i\theta_1}). \tag{75}$$

Here $\theta_1=(2K-k)b_0-ka_0$ and $\theta_2=(2K+k)(a_0+b_0)$. Using this transfer matrix, the multichannel transmission coefficients have been calculated. The transmission probabilities obtained, as functions of the incident intensity $|\mathcal{E}_0|$, are shown in Figs. 17(a)–17(c), for $n=10$, $a_0=b_0=0.5$, $\epsilon_1=1.2$, $\epsilon_2=2.5$, and different values of k_0c. Incident intensity cutoffs are predicted. This could be related to power limiting as suggested in Ref. 23.

B. Multichannel transmission through [GaAs/(δ-scatterer layer)]^n superlattices

In order to study simple examples of multichannel transport processes, let us consider a 3D superlattice $BABAB\ldots ABAB$, where B is a thick semiconducting layer and A is a kind of monoatomic layer, modeled as a plane of attractive or repulsive δ-scatterer centers; see Fig. 18. Assuming the periodic potential

$$V_P(x,y,z)=\gamma\delta(z-\eta l_c)\sum_{\nu=1}^{N_\nu}\sum_{\mu=1}^{N_\mu}\delta(x-x_\nu)\,\delta(y-y_\mu),$$

$$\eta=1,\ldots,n, \tag{76}$$

with longitudinal lattice parameter l_c and interaction strength γ, one can easily obtain the channel coupling parameter

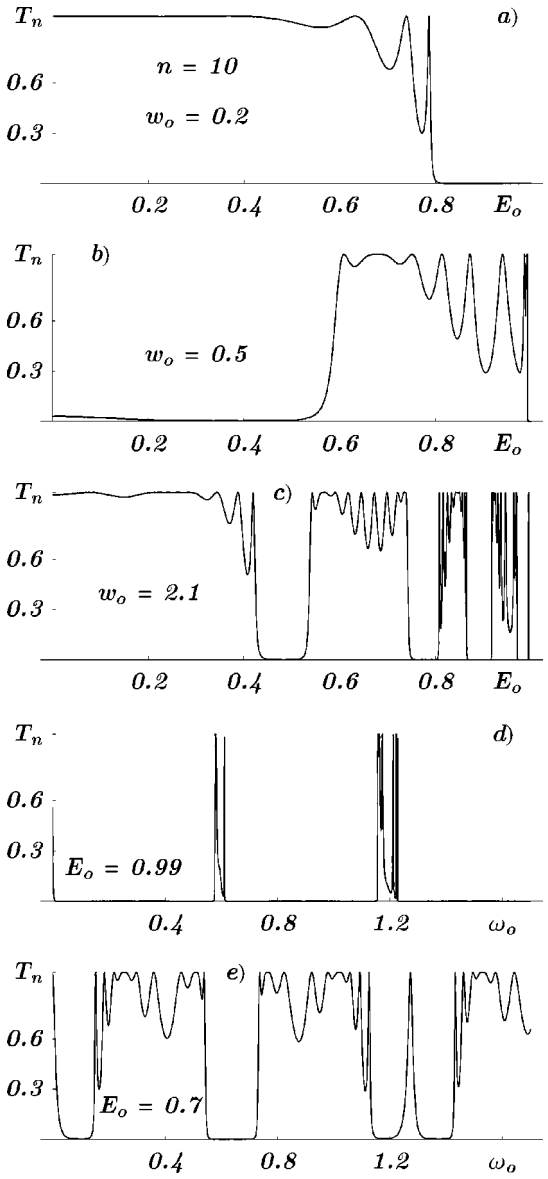

FIG. 17. All graphs in this figure correspond to an optical heterostructure with $n=12$. In (a), (b), and (c) the transmission coefficients are plotted as functions of the incident field intensity $|\mathcal{E}_0|$, for different field frequencies ω_0. Varying this parameter we can find different band structures. An interesting result is the wide gap when $\omega_0=0.5$. In (d) and (e) the band structure as a fuction of the frequency, for fixed incident field intensity $|\mathcal{E}_0|$, has interesting and distinct features.

$$K_{ij}=\frac{8\pi^2 m\gamma}{h^2}\delta(z-\eta l_c)\sum_{\nu=1}^{N_\nu}\sum_{\mu=1}^{N_\mu}\phi_i^*(x_\nu,y_\mu)\phi_j(x_\nu,y_\mu)$$
$$=\delta(z-\eta l_c)\Gamma_{ij}, \tag{77}$$

where the i channel index refers to any pair of quantum numbers $n_x,n_y=1,2,3,\ldots$ in the wave function $\phi_{n_x n_y}(x,y)$, corresponding to the transverse energy levels

$$E_i=\frac{\hbar^2\pi^2}{2m^*}\left(\frac{n_x^2}{w_x^2}+\frac{n_y^2}{w_y^2}\right). \tag{78}$$

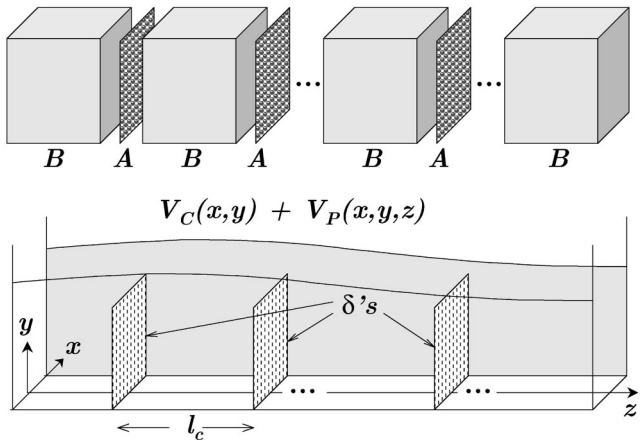

FIG. 18. A soluble multichannel superlatice $BABAB\ldots ABAB$, where monoatomic layers A (modeled as 2D arrays of attractive or repulsive δ-scatterer centers) alternate with dicker semiconductor layers B.

The channel states of Eq. (3),

$$\phi_i(x,y)=\frac{2}{\sqrt{w_x w_y}}\sum_{\{n_i^2=n_x^2+n_y^2\}}\sin\frac{n_x\pi x}{w_x}\sin\frac{n_y\pi y}{w_y}, \tag{79}$$

are either nondegenerate or doubly degenerate states. Taking into account these definitions, and proceeding as usual with δ potentials, it is easy to determine the δ-layer (time-reversal-invariant and flux-conserving) transfer matrix

$$M_\delta=\begin{pmatrix}\alpha_\delta & \beta_\delta\\ \beta_\delta^* & \alpha_\delta^*\end{pmatrix}, \tag{80}$$

with

$$\alpha_\delta=I_N+\beta_\delta,\quad \beta_\delta=\frac{1}{2i}\begin{pmatrix}\frac{\Gamma_{11}}{k_1} & \frac{\Gamma_{12}}{k_1} & & \\ \frac{\Gamma_{21}}{k_2} & \frac{\Gamma_{22}}{k_2} & & \\ & & \ddots & \\ & & & \ddots\end{pmatrix},\quad \frac{\Gamma_{ij}}{\Gamma_{ji}}=\frac{k_i}{k_j}. \tag{81}$$

Although we will obtain here various results for an arbitrary number of channels, N, to evaluate the transmission coefficients T_{ij}, we shall restrict ourselves to $N=2$ and $N=3$ open channels or propagating modes.

To use the polynomials and invariant functions mentioned above, it is necessary to determine the eigenvalues of the $2N\times 2N$ transfer matrix M and to evaluate the matrix polynomials. To this purpose, we need first to obtain the unit-cell transfer matrix. A unit cell of our superlattice contains a layer A and a layer B, which we find convenient to build as a half-layer B followed by the plane of δ-scatterer centers and again a half-layer B, i.e., $B^{1/2}AB^{1/2}$. Thus the single-cell transfer matrix is given by

$$M = W^{1/2} M_{\delta} W^{1/2} = \begin{pmatrix} \alpha & \beta \\ \beta^* & \alpha^* \end{pmatrix}, \tag{82}$$

with

$$W = \begin{pmatrix} \omega & 0 \\ 0 & \omega^* \end{pmatrix}, \quad \omega = \begin{pmatrix} e^{ik_1 b} & 0 \\ 0 & e^{ik_2 b} \\ & & . \end{pmatrix}. \tag{83}$$

It is easy to verify that in this case

$$\beta = \omega^{1/2} \vartheta i \xi \vartheta^T (\omega^*)^{1/2}, \tag{84}$$

with ξ diagonal and ϑ an orthogonal $N \times N$ matrix. Defining appropriate unitary matrices $u = \omega^{1/2}\vartheta$ and $v = -iu^T$, we get, as could be expected, a realization of Bargmann's representation, i.e., $\beta = u \sinh \chi v^*$ with

$$\sinh \chi = \xi = \begin{pmatrix} \xi_1 & & & \\ & \xi_2 & & \\ & & . & \\ & & & . \end{pmatrix}. \tag{85}$$

It is not difficult to show that the transfer-matrix eigenvalues are given, in this case, by

$$\lambda_j = \cosh \chi_j + \sinh \chi_j = \sqrt{1+\xi_j^2} + \xi_j ,$$

$$\lambda_{j+N} = \cosh \chi_{j+N} - \sinh \chi_{j+N} = \sqrt{1+\xi_j^2} - \xi_j . \tag{86}$$

To plot these functions, we assume that the δ-scatterer centers in the x-y plane are located in a square lattice. If we write the functions $\phi_{n_i}(x_\nu, y_\mu)$ as

$$\phi_{n_i}(x_\nu, y_\mu) = \frac{2}{\sqrt{w_x w_y}} \sin\left[\frac{n_x \pi}{\mathcal{N}_\nu}(\nu - x_1)\right] \sin\left[\frac{n_y \pi}{\mathcal{N}_\mu}(\mu - y_1)\right],$$

with x_1 and y_1 the coordinates of the δ center nearest to the origin, it is easy to see that the coupling parameters Γ_{ij} in Eq. (77) depend strongly on the coordinates x_1, y_1.

Let us now evaluate transmission probabilities $|t_{Nn,ij}|^2$ for some specific cases. In Figs. 19(a)–19(c) and 20(a)–20(d), these quantities are plotted for the two-channel case ($N=2$). In Figs. 21 and 22, we consider a larger number of propagating modes ($N>2$). To simplify the notation, the n-cell transmission coefficients $(T_n)_{i,j}$ are denoted just as $T_{i,j}$.

Since some of the multiple features characteristic of the multichannel processes can already be observed in the two-channel case, we shall start discussing this system. For the superlattice that we have just introduced, let us consider two particular cases, differentiated mostly by their interaction strength signs. In both cases we will concentrate on the channel coupling effects. While in Fig. 19 the coupling effects are observed basically at energies below the channel threshold E_{th2} (with negligible band distortion), in Fig. 20 strong band distortions are observed. For the superlattice with transmission coefficients shown in Fig. 19, we have $l_c = 20$ Å, $w_x = w_y = 40$ Å, $x_{\nu 1} = 1/3$, $y_1 = 1/7$, $\mathcal{N}_\nu = \mathcal{N}_\mu = 6$ (meaning 36 δ-scatterer centers for each δ layer), and $\gamma = -500$ eV. For the transmission coefficients in Fig. 20 we consider $l_c = 20$ Å, $w_x = 100$ Å, $w_y = 50$ Å, $x_1 = y_1 = 1/2$, $\mathcal{N}_\nu = 30$, $\mathcal{N}_\mu = 15$ (meaning 450 δ-scatterer centers for each δ layer), and $\gamma = 800$ eV.

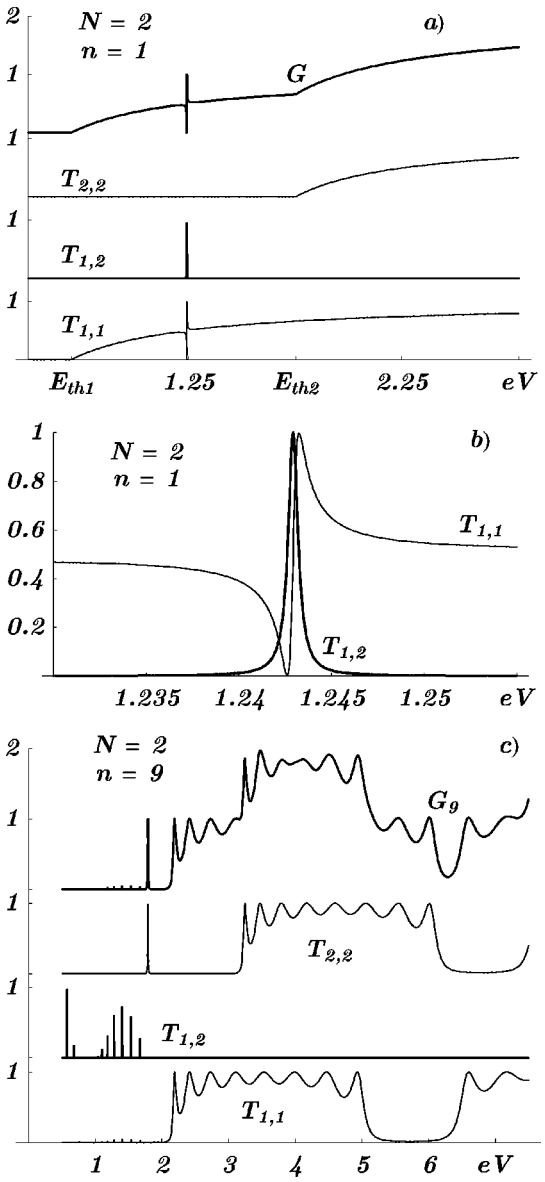

FIG. 19. Total and partial transmission coefficients in the two-channel case ($N=2$), for *attractive* δ-scatterer centers ($\gamma<0$). In (a) and (b), $n=1$ and an isolated resonance, above the channel 1 threshold E_{th1} and below E_{th2}, is produced by coupling between an open and a bounded evanescent state (in the continuum). The resonance at $E=1.242$ eV is magnified and plotted in (b). The strong suppression in T_{11} is accompanied by a resonant behavior of T_{12} that can be fitted quite well with a Lorenzian function. As the number of cells, n, grows [see graph (c)] for $n=9$ the resonance splits off generating a band of resonances.

It is interesting to see that for the *attractive* δ-scatterer centers ($\gamma<0$), very nice resonances, with typical resonance shape and features, appear because of the coupling between an open and an evanescent state [see Fig. 19(b)]. The reso-

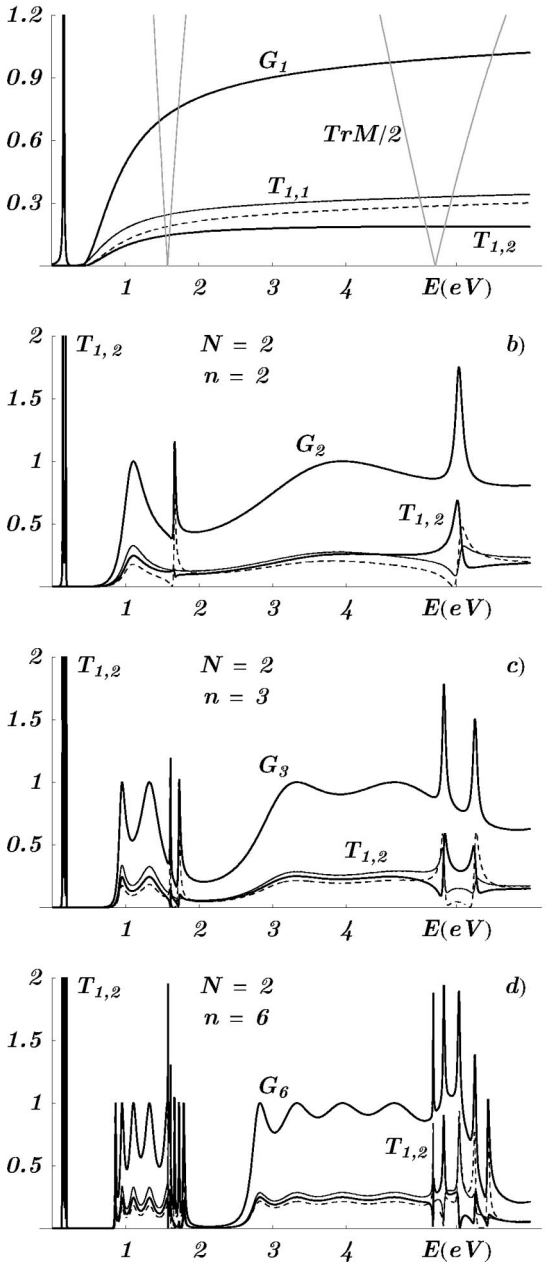

FIG. 20. Two-channel system and the coupling effects on the transmission coefficients T_{ij} above the channel thresholds and for different number of cells, n. As in the previous figure, interesting resonant couplings can be seen. In (c), at $E=4.5$ eV, a complete suppression in the ''elastic'' transmission coefficient T_{ii} is accompanied by strong resonances in the transition coefficients T_{ij}.

nance at $E=1.242$ eV, in Fig. 19(a), is redisplayed in Fig. 19(b). A strong suppression in $T_{1,1}$ is accompanied by a resonant behavior of $T_{1,2}$. This resonance has been normalized and can be fitted with a Lorenzian function, as is well known in scattering theory. The lifetime of the quasistationary resonant states, given by the resonance width, becomes larger as the number of cells, n, increases. Simultaneously, as n increases the resonance splits off generating, due to phase coherence phenomena, a band of resonances [see the low-energy region of Fig. 19(c)].

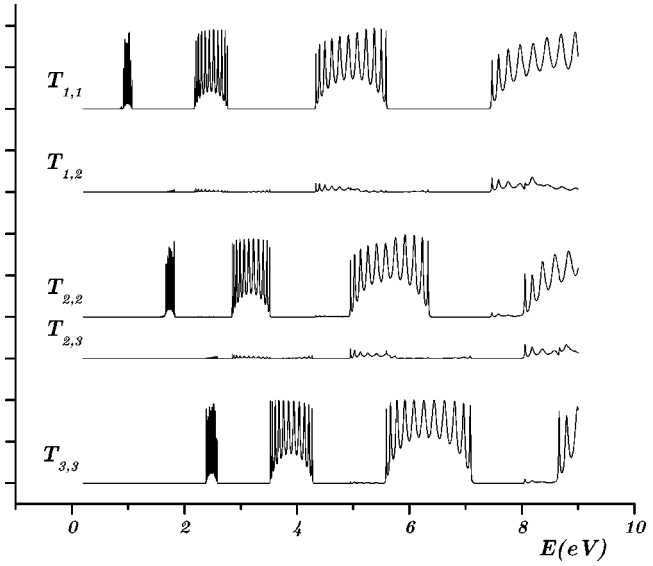

FIG. 21. Three propagating channels and their transmission coefficients. In this graphs a small coupling allows one to recognize the uncoupled band structure for channels 1, 2, and 3. The channel coupling induces transitions from channel i to channel $j\neq i$ even if the energy lies in the gap of one of them.

The system whose transmission coefficients have been plotted in Fig. 20 contains planes of *repulsive* δ-scatterer centers. Although at very small energies ($<E_{th1},E_{th2}$) we also find a channel-coupling resonance (indicated with $T_{1,2}$), the transmission probability from channel 1 to channel 2 becomes larger than for the attractive δ's above the energy thresholds E_{th1} and E_{th2}. For the parameter values chosen in this case $T_{1,2}$ is comparable in magnitude with $T_{1,1}$ and $T_{2,2}$. In some cases strong suppressions in the transmission coefficients $T_{1,1}$ and $T_{2,2}$ are observed, with no influence on the total transmission probability or conductance $G_n=\mathrm{Tr}\, t_n t_n^{\dagger}$. For this reason, it is clear that this type of effects will remain unobserved, at least while the experimental techniques cannot efficiently discriminate one channel from another. Besides the band distortion, other significant features are also apparent. At the incoming particle energy of 4.6 eV in Fig. 20(c), the transition coefficients $T_{1,2}$ and $T_{2,1}$ contribute to the largest value of the conductance G_3, while $T_{1,1}=T_{2,2}$ becomes zero. In Fig. 20(a), the transfer-matrix trace has been also plotted and, as in the one propagating mode case, it indicates the regions of allowed and forbidden energies.

It is interesting to notice that the channel-mixing effects, measured by the relative size of $T_{1,2}$, become larger as the system's size $L=nl_c$ increases.

In Figs. 21 the transmission coefficients $T_{i,j}$ are plotted for $N=3$. In these figures we have considered $l_c=16$ Å, $\gamma=0.4$ keV, and $x_1=y_1=1$ (with $w_x=w_y=24$ Å and $\mathcal{N}_\nu=\mathcal{N}_\mu=6$). A physically interesting property that can be very clearly observed is the *return effect*, occurring when a particle comes out in the same channel of the incoming one but having passed, at least once, through another propagating mode. Because of this effect, the band structure of $T_{i,i}$ is modified in the energy regions where the allowed energy band of channel k coincides with the forbidden energy band

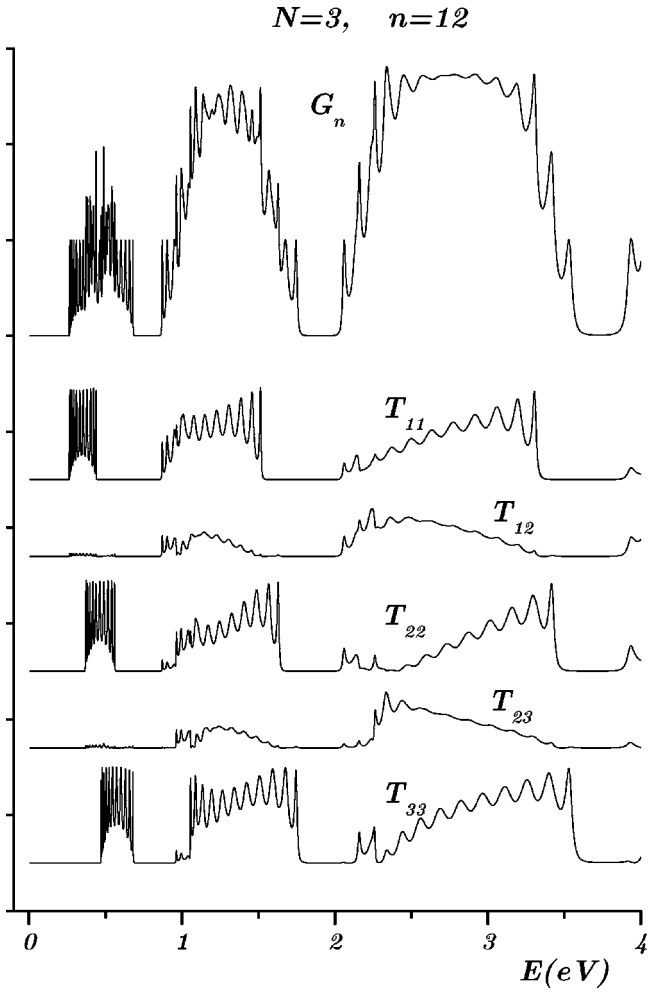

FIG. 22. Strong coupling of three propagating channels and the effects in their transmission coefficients. All the transmission coefficients, except the total transmission coefficient or conductance, are strongly modified especially for energies in the third band. Looking carefully at the energy region between 2 and 2.5 eV we can see, for example, that a particle coming in channel 3 leaves also in channel 3 after having passed through the other two channels.

of channel i and whenever the transition probability $T_{i,k}$ takes non-negligible values. Consider, for example, the graphs for $T_{1,1}$, $T_{1,2}$, and T_{22}. The *transition* probability $T_{1,2}$ is different from zero in the energy regions corresponding to allowed bands of both $T_{1,1}$ and $T_{2,2}$. If we observe now the transmission coefficient $T_{2,2}$ in the gap between the third and fourth bands, there is a small probability for the particle to start and finish in the same channel 2 for energies in the allowed band of channel 1 and the forbidden energies of channel 2. This is possible if the particle enters in channel 2, passes to channel 1, and, before reaching the end of the superlattice, comes back to channel 2. In these graphs we can also see that T_{11} and T_{22} do not reach the maximum value of 1 in their allowed energy bands.

If we observe the transmission coefficients in Fig. 22, the return effect is much more pronounced because the transition coefficients $T_{i,j}$ take values comparable with those of $T_{i,i}$. This effect is apparent in, say, $T_{2,2}$ for energies around 1, 0, and 2.2 eV, corresponding to the second and third energy bands. At these energies, the particle starts in channel 3 and finishes in the same channel but passing through channel 2 or, perhaps, also through channel 1. This type of experimental information, even for the two-channel problems, is not yet available. We expect that such quantities will be measured soon, because they will give more insight into the tunneling mechanism and on the way the flux of certain kinds of quasiparticles moves from one channel to another. It is worth mentioning that this effect depends also on the superlattice size and layers widths. Some calculations and also applications are in progress.

The channel coupling parameters Γ_{ij} are important quantities that are strongly dependent on the periodic potential ability to induce flux interchange between the various propagating modes. In the model considered here, they can easily be calculated for any configurations of δ's. For different distributions, distinct and interesting band-mixing effects are predicted. In other kind of problems—say, spin-dependent problems—incoming particles may emerge on the other side with their spin reversed.[36] By the same token, heavy holes transform into light holes. The uncoupled-channel limit resonances of the ith mode may be present or absent when the coupling is turned on. Resonances associated with the uncoupled kth (with $k \neq i,j$) channel can be present in $(T_n)_{ij}$. Expected and nonexpected phenomena of suppression, *broadening*, enhancement, and apparent *generation of new transmission resonances, produced by interchannel couplings*, are of primary importance and offer the possibility of modeling and predicting novel tunneling effects and interference phenomena.

VI. CONCLUSIONS

Theoretical developments and various physical properties of finite periodic systems have been discussed from the point of view of the transfer matrix and the scattering theory. In this theory, alternative to the current solid state theory, the principal features of the real periodic sytems—finiteness and periodicity—are fully incorporated without any need for Bloch functions and reciprocal space. While in the standard theory one works, by construction, in the continuous spectrum limit (of infinite systems) in this approach we have complete control of the system's size and the entire phase coherence phenomena. As a consequence, one can easily determine the fundamental phase interference effects as well as the discrete character of the energy spectrum, emblematic of finite systems. Using simple, algebraic methods, universal, extremely simple and compact expressions for global n -cell quantities, valid for any realization of the potential function, have been rigorously and directly obtained.

The scattering approach, which up until now has successfully dealt with transport properties of disordered and chaotic structures, used properly, can also give information on the innards of finite periodic systems. From the transmission coefficients we get information on the band structure and, even more, on the intraband structure and on the resonant energies. This information opened up the possibility of evaluat-

ing and describing extended, resonant, and localized states inside the periodic systems. For multichannel systems, we have also shown that it is possible to evaluate resonant channel couplings and to get insight into the particle's excursions through the space of open and evanescent channels.

From the transfer-matrix combination property $M_n = MM_{n-1}$ we deduced recurrence relations for the submatrices α_n and β_n. These relations were used both to derive new formulas for global scattering amplitudes and quantum properties and to deduce *matrix recurrence relations* whose solutions are the noncommutative polynomials $p_{N,n}$. These, in the 1D one-channel limit, are the well-known Chebyshev polynomials of the second kind.

A highly peculiar and significant property of the general expressions describing the physics of *n*-cell system with an arbitrary number of propagating modes *N* and arbitrary single-cell potential function is the consistent presence of the two fundamental quantum properties: the tunneling effect and the phase coherence. The tunneling process is generally expressed by the single-cell matrix elements or the single cell scattering amplitudes. The multiple reflection and interference phenomena, occurring along *n* repetitions of the single cell and between the various channels, is described in these formulas by means of the polynomials $p_{N,n}$. In this sense, the theory presented in this paper not only generalizes the one-channel descriptions to provide extremely simple formulas for the transmission coefficients of *n*-layer *N*-channel systems, but also gives more general, simple, precise descriptions of some fundamental qualitative properties. The position and widths of the allowed bands are given by the trace of the single-cell transfer matrix, the tunneling resonances by the zeros of the polynomials $p_{N,n}$.

Some *few-channel* examples have been considered. We started by studying nonspecific properties common to all 1D one-channel finite periodic systems. To this purpose we used the Bargmann parameters to express the physical quantities. Based on this analysis we could make clear that the phase coherence phenomena are responsible for the universal band structure behavior. Specific examples were also considered, and the square- and δ-barrier potentials were frequently used to illustrate and perform explicit calculations. We have shown that in the limit $n \to \infty$, the square-barrier system is obviously the Kronig-Penney model. Band structure tailoring has also been discussed. Playing with a few potential parameters, interesting effects and some well-known properties were found both for donorlike and acceptorlike ''impurities'' or topological defects. We have shown that easier impurity calculations can be done using this method and that the isolated impurity levels or minibands in the energy gaps can be located almost at will. We also applied our method to multilayer quasilinear optical systems and quantum dot arrays (not reported here) with equal feasibility and success.

A short discussion of simple but illustrative *two- and three-channel* systems was also presented. To illustrate the analysis of this type of system, we considered a soluble multichannel superlatice $BABAB \ldots ABAB$, where monoatomic layers *A* alternate with thicker semiconductor layers *B*. For attractive δ potentials, faithful resonances appear because of the coupling between open and evanescent states. For repulsive δ potentials, an interesting *return effect* is clearly recognized when a particle comes out in the same channel as the incoming one but having passed, at least once, through another propagating mode. Many other properties, such as resonance broadenings, suppressions, and channel mixings, are observed in general. The lateral dimensions w_x, w_y, the cell length l_c, the number of δ's per plane, and their distribution have important consequences in the transmission coefficients.

In conclusion we presented here an alternative and convenient method to study some properties in solid-state physics.

ACKNOWLEDGMENTS

The authors gratefully acknowledge Professor H. Simanjuntak, Professor A. Robledo, Professor J. Grabinsky, and Professor R. Perez-Alvarez for useful and clarifying comments and CONACyT Mexico (Project No. E-29026). This work was done within the framework of the Associateship Scheme of the Abdus Salam International Center for Theoretical Physics, Trieste Italy.

APPENDIX A: THE TRANSFER MATRIX IN THE KRONIG-PENNEY MODEL

For the benefit of those who are not familiar with the transfer-matrix method, let us consider a simple example, the finite Kronig-Penney model, and calculate the single-cell transfer matrix. A sectionally constant potential profile of this type might correspond to the conduction- or valence-band edge of a superlattice $(AB)^n$, in which case the effective masses in the alternating layer should be considered. In this case, the current or flux conservation requirement must be considered. In the valley region *A* of this system, the wave function is

$$\psi_A(z) = a_A e^{ikz} + b_A e^{-ikz} \equiv a_A \vec{\varphi}(z) + b_A \overleftarrow{\varphi}(z), \quad \text{(A1)}$$

where $k = \sqrt{(2m_A/\hbar^2)E}$, while in the barrier regions *B*, with $\kappa = \sqrt{(2m_B/\hbar^2)(V_0 - E)}$ for $E < V_0$, the wave function is

$$\psi_B(z) = a_B e^{\kappa z} + b_B e^{-\kappa z} \equiv a_B \varphi^+(z) + b_B \varphi^-(z). \quad \text{(A2)}$$

The continuity conditions at the interface points z_l and $z_r = z_l + b_0$, at the left- and right-hand sides of barrier *B*, can be written as

$$\begin{aligned} \phi_B(z_l^+) &= \begin{pmatrix} a_B e^{\kappa z_l^+} \\ b_B e^{-\kappa z_l^+} \end{pmatrix} \\ &= \frac{1}{2\kappa} \begin{pmatrix} \kappa + ik & \kappa - ik \\ \kappa - ik & \kappa + ik \end{pmatrix} \begin{pmatrix} a_A e^{ikz_l^-} \\ b_A e^{-ikz_l^-} \end{pmatrix} \\ &\equiv M_{i0}(z_l^+, z_l^-)\, \phi_A(z_l^-) \end{aligned} \quad \text{(A3)}$$

and

$$\phi_A(z_r^+)=\begin{pmatrix} a_A e^{ikz_r^+} \\ b_A e^{-ikz_r^+}\end{pmatrix}=\frac{1}{2k}\begin{pmatrix} k-i\kappa & k+i\kappa \\ k+i\kappa & k-i\kappa\end{pmatrix}\begin{pmatrix} a_B e^{\kappa z_r^-} \\ b_B e^{-\kappa z_r^-}\end{pmatrix}$$
$$\equiv M_{0i}(z_r^+,z_r^-)\phi_B(z_r^-). \tag{A4}$$

It is not difficult to show that the current conservation requirements

$$j(z_l^+)=j(z_l^-),\quad j(z_r^+)=j(z_r^-)$$

imply the conditions

$$M_{i0}^\dagger\begin{pmatrix} 0 & 1 \\ -1 & 0\end{pmatrix}M_{i0}=-\frac{ikm_B}{\kappa m_A}\begin{pmatrix} 1 & 0 \\ 0 & -1\end{pmatrix},$$

$$M_{0i}^\dagger\begin{pmatrix} 1 & 0 \\ 0 & -1\end{pmatrix}M_{0i}=-\frac{i\kappa m_A}{km_B}\begin{pmatrix} 0 & 1 \\ -1 & 0\end{pmatrix}.$$

The transfer matrices here connect the state vectors in the outside with the state vectors inside the square-barrier potential. State vectors at any two points of a constant potential region differ in their phases and are also related by a transfer matrix. For z_a and z_a' in the valley region A, we have

$$\phi_A(z_a')=\begin{pmatrix} e^{ik(z_a'-z_a)} & 0 \\ 0 & e^{-ik(z_a'-z_a)}\end{pmatrix}\phi_A(z_a)$$
$$=M_A(z_a',z_a)\phi_A(z_a), \tag{A5}$$

and for z_b and z_b' in the barrier region, we have

$$\phi_B(z_b')=\begin{pmatrix} e^{\kappa(z_b'-z_b)} & 0 \\ 0 & e^{-\kappa(z_b'-z_b)}\end{pmatrix}\phi_B(z_b)$$
$$=M_B(z_b',z_b)\phi_B(z_b). \tag{A6}$$

Using the multiplicative property, it is possible to obtain the transfer matrix relating any two points of the superlattice. The state vectors at any z_a (in the valley A) and z_b (in the neighbor barrier region B) are related by

$$\phi_B(z_b)=M_B(z_b,z_l^+)M_{i0}(z_l^+,z_l^-)M_A(z_l^-,z_a)\phi_A(z_a)$$
$$=M_{ba}(z_b,z_a)\phi_A(z_a). \tag{A7}$$

The current conservation requirement

$$j(z_a)=j(z_b)$$

implies the condition

$$M_{ba}^\dagger\begin{pmatrix} 1 & 0 \\ 0 & -1\end{pmatrix}M_{ba}=-\frac{i\kappa m_B}{km_A}\begin{pmatrix} 0 & 1 \\ -1 & 0\end{pmatrix}. \tag{A8}$$

In the same way, the matrix relating the state vectors $\phi_A(z_l^-)$ and $\phi_A(z_r^+=z_l^-+b_0)$, at the left- and right-hand sides of the square barrier, is obtained from

$$M_b(z_l^-+b_0,z_l^-)=M_{0i}(z_r^+,z_r^-)M_B(z_r^-,z_l^+)M_{i0}(z_l^+,z_l^-).$$

Therefore

$$M_b(z_l^-+b_0,z_l^-)=\begin{pmatrix} \cosh\kappa b_0+i\dfrac{k^2-\kappa^2}{2k\kappa}\sinh\kappa b_0 & -i\dfrac{k^2+\kappa^2}{2k\kappa}\sinh\kappa b_0 \\ i\dfrac{k^2+\kappa^2}{2k\kappa}\sinh\kappa b_0 & \cosh\kappa b_0-i\dfrac{k^2-\kappa^2}{2k\kappa}\sinh\kappa b_0\end{pmatrix}. \tag{A9}$$

It is easy to show that the current conservation $j(z_l^-)=j(z_r^+)$ leads to the well-known FC requirement

$$M_b^\dagger\begin{pmatrix} 1 & 0 \\ 0 & -1\end{pmatrix}M_b=\begin{pmatrix} 1 & 0 \\ 0 & -1\end{pmatrix}. \tag{A10}$$

APPENDIX B: THE BARGMANN REPRESENTATION

The transfer matrix of the orthogonal universality class M_0 belongs to the symplectic $\mathrm{Sp}(2N,\mathcal{C})$ group, with $(2N^2+N)$ free parameters, while the transfer matrix in the unitary universality class M_u belongs to the pseudounitary $\mathrm{psU}(2N,\mathcal{C})$ group, with $(4N^2+N)$ free parameters. Most of the transfer matrices appearing in the literature belong to these groups.

Sometimes, it may be *convenient*, but it is not essential for this theory, to express the transfer matrices in the so-called Bargmann representation[20]

$$M_0=\begin{pmatrix} u & 0 \\ 0 & u^*\end{pmatrix}\begin{pmatrix} \cosh\chi & \sinh\chi \\ \sinh\chi & \cosh\chi\end{pmatrix}\begin{pmatrix} v & 0 \\ 0 & v^*\end{pmatrix} \tag{B1}$$

and

$$M_u=\begin{pmatrix} u_1 & 0 \\ 0 & u_2\end{pmatrix}\begin{pmatrix} \cosh\chi & \sinh\chi \\ \sinh\chi & \cosh\chi\end{pmatrix}\begin{pmatrix} v_1 & 0 \\ 0 & v_2\end{pmatrix}, \tag{B2}$$

with u's and v's unitary matrices and χ diagonal and positive. In this representation, the transfer-matrix blocks take simple functional forms. In the orthogonal case we have

$$\alpha=u\cosh\chi v^\dagger,$$

$$\beta=u\sinh\chi v^T. \tag{B3}$$

The Bargmann parameters are well-defined functions of the energy E and other potential parameters in a way which depends on the particular physical system. For the familiar 1D

Kronig-Penney model shown in Fig. 3, the Bargmann parameters χ and $\phi \equiv \phi_u - \phi_v$ are given by

$$\chi = \cosh^{-1}\left[1 + \frac{v_0^2}{\epsilon(\epsilon - v_0)} \sinh^2\left(\frac{\sqrt{2m_b^*(\epsilon - v_0)}}{\hbar}\right)^{1/2}\right] \tag{B4}$$

and

$$\phi = \frac{\sqrt{2m_v^*\epsilon}}{\hbar}\left(1 + \frac{a_0}{b_0}\right) + \tan^{-1}\left[\frac{2\epsilon - v_0}{\sqrt{\epsilon(\epsilon - v_0)}} \tanh\left(\frac{\sqrt{2m_b^*(\epsilon - v_0)}}{\hbar}\right)\right]. \tag{B5}$$

When the square-barrier potential is due to alternating semiconductor layers, we have m_v^* and m_b^* as the effective masses in the valley and barrier, respectively. In the previous formulas, we have considered also the parameters $\epsilon = Eb_0^2$ and $v_0 = V_0 b_0^2$. We shall use χ and ϕ to discuss the relation between the Chebyshev polynomials and the resonant transmission and reflection interference phenomena, keeping the analysis as general as possible. The Bargmann parameters can also be used to make clear some potential-independent features such as the deep relation between the band structure and the phase coherence phenomena in periodic systems, discussed in Sec. V.

APPENDIX C: RELATIONS BETWEEN THE SCATTERING AND THE TRANSFER MATRIX

Explicit relations between the transfer and scattering matrix elements are known; see, for example, Ref. 22. For scattering processes like the one sketched in Fig. 2, the coefficients r, t, r', and t' are the reflection and transmission amplitudes corresponding to incident particles coming from the left- and right-hand sides, respectively. The scattering matrix S, which relates the incident amplitudes a and d with the outgoing amplitudes $b = ra + t'd$ and $c = ta + r'd$, is written as

$$S = \begin{pmatrix} r & t' \\ t & r' \end{pmatrix}. \tag{C1}$$

Let us consider the transfer matrix of the unitary universality class M_u. For TRI systems, we have to take $\gamma = \beta^*$ and $\delta = \alpha^*$, and based on the scattering and transfer-matrix definitions, one easily obtains the following equations:

$$\begin{aligned} t - \alpha - \beta r &= 0, \\ r' - \beta t' &= 0, \\ \gamma + \delta r &= 0, \\ 1 - \delta t' &= 0, \end{aligned} \tag{C2}$$

whose solutions [with the dagger (†) meaning the transpose conjugate] are[22]

$$r = -\delta^{-1}\gamma = -v_2^\dagger (\tanh\chi) v_1, \tag{C3}$$

$$t = (\alpha^\dagger)^{-1} = u_1 (\cosh\chi)^{-1} v_1, \tag{C4}$$

$$t' = \delta^{-1} = v_2^\dagger (\cosh\chi)^{-1} u_2^\dagger, \tag{C5}$$

$$r' = \beta\delta^{-1} = u_1 (\tanh\chi) u_2^\dagger. \tag{C6}$$

Thus, the transfer matrix of the unitary universality class can be written as

$$M_u = \begin{pmatrix} (t^\dagger)^{-1} & r'(t')^{-1} \\ -(t')^{-1} r & (t')^{-1} \end{pmatrix}, \tag{C7}$$

while in the orthogonal universality class it takes the form

$$M_0 = \begin{pmatrix} (t^\dagger)^{-1} & r^*(t^T)^{-1} \\ (t^T)^{-1} r & (t^T)^{-1} \end{pmatrix}. \tag{C8}$$

The explicit parametrizations appearing on the right-hand sides of Eqs. (C3)–(C6) correspond to Bargmann's representation.

APPENDIX D: MRR AND THE CAYLEY-HAMILTON THEOREM

It is not difficult to recognize that the *noncommutative polynomial recurrence relation*

$$p_n^{(i)} + \zeta_i p_{n-1}^{(i)} + \eta_i p_{n-2}^{(i)} = 0 \quad \text{for } n \geqslant 1 \quad \text{and } i = 1,2, \tag{D1}$$

where $\zeta_1 = -(\beta^{-1}\alpha\beta + \delta)$ and $\eta_1 = (\delta\beta^{-1}\alpha\beta - \gamma\beta)$ are the matrix coefficients for the unitary class, and $\zeta_2 = -(\beta^{-1}\alpha\beta + \alpha^*)$ and $\eta_2 = (\alpha^*\beta^{-1}\alpha\beta - \beta^*\beta)$ the matrix coefficients for the orthogonal class, transforms into the *scalar recurrence relation*

$$\beta_{n+2N}^{i,j} + g_1\beta_{n+2N-1}^{i,j} + \cdots + g_{2N-1}\beta_{n+1}^{i,j} + g_{2N}\beta_n^{i,j} = 0, \quad \forall\ i,j \text{ and } n \neq 0 \tag{D2}$$

and similar relations for $\alpha_m^{i,j}$, $\gamma_m^{i,j}$, and $\delta_m^{i,j}$. Equation (D1) is the Cayley-Hamilton theorem for M.[37] The coefficients g_m are precisely those of the characteristic polynomial of M, defined by Leverrier's algorithm,[38] being $g_1 = -\mathrm{Tr}\, M$ and $g_{2N} = \det M$. Taking into account that the recurrence relation holds irrespectively of the indices i,j, we write

$$\pi_{n+2N} + g_1\pi_{n+2N-1} + \cdots + g_{2N-1}\pi_{n+1} + g_{2N}\pi_n = 0, \tag{D3}$$

with the initial conditions $\pi_0 = I_N$, for $\pi = \alpha, \delta$, $p_N^{(1)}$, $p_N^{(2)}$, or $\pi_0 = 0$, for $\pi = \beta, \gamma$. Since $p_{N,m}^{(1)}$ and $p_{N,m}^{(2)}$ are formally equal, we have to deal with only one set of polynomials which satisfy the relation

$$p_{N,n+2N} + g_1 p_{N,n+2N-1} + \cdots + g_{2N-1}p_{N,n+1} + g_{2N}p_{N,n} = 0 \quad \text{for } n \geqslant 0. \tag{D4}$$

Notice that the same equation is valid in the orthogonal universality class, differing only in the explicit form of the coefficients g_m. The polynomials $p_{N,m}$ are in some respect universal quantities. Solving for p_n, we will be ready to determine α_n, β_n, γ_n, and δ_n, and subsequently to evaluate the superlattice physical quantities of interest for multilayer systems. This is one of our main goals.

APPENDIX E: THE CHEBYSHEV AND THE NONCOMMUTATIVE POLYNOMIALS

1. one-channel case

To introduce the procedure to solve the most general case using the well-known generating function method and to introduce a notation we start by recalling the well-known Chebyshev relation

$$p_n+g_1p_{n-1}+p_{n-2}=0, \tag{E1}$$

with $p_{-1}=0$, $p_0=1$, and

$$g_1=-\mathrm{Tr}\,M. \tag{E2}$$

Schematically, we can proceed as follows.

(i) Developing the generating function $g(\lambda)=(1+g_1\lambda+g_2\lambda^2)^{-1}$ around $\lambda=0$, one has

$$\frac{1}{1+g_1\lambda+g_2\lambda^2}=q_0+q_1\lambda+q_2\lambda^2+q_3\lambda^3+\cdots, \tag{E3}$$

where

$$q_0=1, \tag{E4}$$

$$q_1+g_1q_0=0, \tag{E5}$$

and

$$q_{n+2}+g_1q_{n+1}+g_2q_n=0 \quad \text{for } n\geqslant 0. \tag{E6}$$

All this is compatible with Eq. (D1). Thus, q_n can be identified with p_n.

(ii) Any combination like

$$q_n=s_1\lambda_1^n+s_2\lambda_2^n, \tag{E7}$$

where λ_1 and λ_2 are the eigenvalues of M, is also a solution of the recurrence relation. To fulfill Eqs. (E6) and (E7), s_1 and s_2 should satisfy the set of equations

$$s_1+s_2=1, \tag{E8}$$

$$s_1(\lambda_1+g_1)+s_2(\lambda_2+g_1)=0, \tag{E9}$$

the solutions of which are (recall that $g_1=-\mathrm{Tr}\,M=-\lambda_1-\lambda_2$)

$$s_1=\frac{\lambda_1}{\lambda_2-\lambda_1}, \quad s_2=\frac{\lambda_2}{\lambda_1-\lambda_2}. \tag{E10}$$

Thus,

$$q_n=\frac{\lambda_1^{n+1}-\lambda_2^{n+1}}{\lambda_2-\lambda_1}=p_n. \tag{E11}$$

This is the well-known Chebyshev polynomial of the second kind in the eigenvalue representation.

2. *N*-channel case

For $N\geqslant 2$, we have the MRR

$$p_{N,n}=-\zeta p_{N,n-1}-\eta p_{N,n-2}, \tag{E12}$$

where $\zeta=-(\beta^{-1}\alpha\beta+\delta)$ and $\eta=(\delta\beta^{-1}\alpha\beta-\gamma\beta)$. This seems complicated but it is a solvable problem. As mentioned before this three-term relation transforms into the scalar recurrence relation (E1) with $2N+1$ terms.

Without loss of generality and assuming that $\lambda_i-\lambda_j\neq 0$, $\forall$ i and j, we can consider the generating function

$$Q(\lambda)=\frac{I_N}{1+g_1\lambda+g_2\lambda^2+\cdots g_{2N}\lambda^{2N}}$$
$$=q_{N,0}+q_{N,1}\lambda+q_{N,2}\lambda^2+\cdots, \tag{E13}$$

whose coefficients $q_{N,i}$ satisfy the following $2N$ conditions:

$$q_{N,0}=I_N, \tag{E14}$$

$$q_{N,1}+g_1q_{N,0}=0, \tag{E15}$$

$$q_{N,2}+g_1q_{N,1}+g_2q_{N,0}=0, \tag{E16}$$

$$\vdots$$

and the recurrence relation

$$q_{N,n+2N}+g_1q_{N,n+2N-1}+\cdots+g_{2N-1}q_{N,n+1}+g_{2N}q_{N,n}$$
$$=0 \quad \text{for } n\geqslant 0. \tag{E17}$$

Except for the first equation and the last recurrence relation, these conditions are not fully compatible with the matrix recurrence relation (E12). For example, recalling that $p_{N,-1}=0$, we have from Eq. (E12)

$$p_{N,1}+\zeta p_{N,0}=0 \quad \text{with } \zeta\neq g_1.$$

Thus, the generating function has to be modified.[21] Before doing that, we shall continue deriving the coefficients $q_{N,n}$, because at the end the general solution depends also on these quantities. Since the $q_{N,n}$ are multiples of I_N, we shall work as if they were scalar quantities and, again, to keep a simple notation we shall also drop the subindex N, which will not appear in our expressions unless the number of channels needs to be specified. If we take the combination

$$q_n=s_1\lambda_1^n+s_2\lambda_2^n+\cdots+s_{2N}\lambda_{2N}^n \tag{E18}$$

and use the previous conditions, the coefficients s_i can be determined by solving the set of equations

$$\sum_{i=1}^{2N} d_{ki}s_i=\delta_{k,0}, \quad k=0,1,\ldots,2N-1, \tag{E19}$$

where

$$d_{ki}=\lambda_i^k+g_1\lambda_i^{k-1}+\cdots+g_{k-1}\lambda_i+g_k. \tag{E20}$$

The coefficients g_m are the well-known symmetric functions

$$g_m=(-)^m\sum_{l_1<l_2<\cdots<l_m}^{2N}\lambda_{l_1}\lambda_{l_2}\cdots\lambda_{l_m},\quad g_0=1. \tag{E21}$$

It is easy to verify that

$$s_i=\frac{\lambda_i^{2N-1}}{\prod_{j\neq i}^{2N}(\lambda_i-\lambda_j)} \tag{E22}$$

and, thus,

$$q_n=\sum_{i=1}^{2N}\frac{\lambda_i^{2N+n-1}}{\prod_{j\neq i}^{2N}(\lambda_i-\lambda_j)}I_N. \tag{E23}$$

To fulfill the MRR, we have to consider a generating function like

$$F(\lambda)=(I+\rho_1\lambda+\rho_2\lambda^2+\cdots+\rho_{2N-1}\lambda^{2N-1})Q(\lambda)$$

$$\equiv\sum_{m=0}p_m\lambda^m, \tag{E24}$$

with ρ_i are $N\times N$ matrices and

$$p_m=\begin{cases}\sum_{k=0}^{m}\rho_k q_{m-k} & \text{when } m\leqslant 2N-1,\\ \sum_{k=0}^{2N-1}\rho_k q_{m-k} & \text{when } m\geqslant 2N \quad W0X.\end{cases} \tag{E25}$$

These matrices satisfy the MRR if

$$\rho_1=p_1+g_1p_0, \tag{E26}$$

$$\rho_2=p_2+g_1p_1+g_2p_0, \tag{E27}$$

$$\rho_{2N-1}=p_{2N-1}+g_1p_{2N-2}+\cdots+g_{2N-1}p_0; \tag{E28}$$

i.e., the polynomials p_m in Eq. (E25) satisfy the MRR when

$$\rho_k=\sum_{l=0}^{k}p_l g_{k-l},\quad \rho_0=1. \tag{E29}$$

Replacing this, we have finally

$$p_{N,m}=\sum_{k=0}^{m}\sum_{l=0}^{k}p_{N,l}g_{k-l}q_{m-k}\ \text{ for }\ m<2N \tag{E30}$$

and

$$p_{N,m}=\sum_{k=0}^{2N-1}\sum_{l=0}^{k}p_{N,l}g_{k-l}q_{m-k}\quad \text{for }\ m\geqslant 2N. \tag{E31}$$

These are precisely the polynomials $p_{N,m}$ we are looking for.

[1] F. Bloch, Z. Phys. **52**, 555 (1928); F. Seitz, *Modern Theory of Solids* (McGraw-Hill, New York, 1940); N. F. Mott and H. Jones, *Theory of the Properties of Metals and Alloys* (Oxford University Press, Oxford, 1936); R. Peierls, *Quantum Theory of Solids* (Oxford University Press, Oxford, 1955); J. M. Ziman, *Principles of the Theory of Solids*, 2nd ed. (Cambridge University Press, Cambridge, England, 1972); C. Kittel, *Introduction to Solid State Physics*, 5th ed. (Wiley, New York, 1976).

[2] O. Maddelung, *Introduction to Solid State Theory*, Springer Series in Solid-State Sciences, Vol. 2 (Springer-Verlag, Heidelberg, 1981); P. Y. Yu and M. Cardona, *Fundamentals of Semiconductors* (Springer-Verlag, Heidelberg, 1996).

[3] V. Mitin, V. A. Kochelap, and M. A. Strocio, *Quantum Heterostructures* (Cambridge University Press, New York, 1999).

[4] P. Pereyra, Phys. Rev. Lett. **80**, 2677 (1998).

[5] R. Tsu and L. Esaki, Appl. Phys. Lett. **24**, 562 (1973).

[6] E. L. Ivchenko and G. E. Pikus, *Superlattices and other Heterostructures, Symmetry and Optical Phenomena*, Springer Series in Solid-State Sciences, Vol. 110 (Springer-Verlag, Heidelberg, 1995).

[7] E. E. Mendez, W. I. Wang, B. Ricco, and L. Esaki, Appl. Phys. Lett. **47**, 415 (1985); L. F. Luo, R. Beresford, and W. I. Wang, *ibid.* **55**, 2023 (1989); E. E. Mendez, H. Ohmo, L. Esaki, and W. I. Wang, Phys. Rev. B **43**, 5196 (1991).

[8] M. Helm, P. England, E. Colas, F. DeRosa, and S. J. Allen, Jr. Phys. Rev. Lett. **63**, 74 (1989); H. T. Grahn, H. Schneider, W. W. Rühle, K. von Klitzing, and K. Ploog, *ibid.* **64**, 3163 (1990).

[9] M. Morifuji and C. Hamaguchi, Phys. Rev. B **52**, 14 131 (1995); P. A. Chen and C. Y. Chang, J. Appl. Phys. **74**, 7294 (1993).

[10] F. Capasso, S. Sen, F. Beltram, and A. Y. Cho, in *Physics of Quantum Electron Devices*, edited by F. Capasso (Springer, Berlin, 1990), pp. 181–182.

[11] M. U. Erdoğan, K. W. Kim, and M.A. Stroscio, Appl. Phys. Lett. **62**, 1423 (1992); L. G. Gerchikov, B. D. Oskotsky, and A. V. Subashiev, Phys. Rev. B **50**, 15 416 (1994).

[12] P. Pereyra (unpublished).

[13] D. J. Griffiths and N. F. Taussing, Am. J. Phys. **60**, 883 (1992).

[14] T. H. Kolatas and A. R. Lee, Eur. Phys. J. B **12**, 275 (1991).

[15] H. W. Lee, A. Zysnarsky, and P. Kerr, Am. J. Phys. **57**, 729 (1989).

[16] D. Kiang, Am. J. Phys. **42**, 785 (1974).

[17] R. Pérez-Alvarez and H. Rodriguez-Coppola, Phys. Status Solidi B **145**, 493 (1988).

[18] D. W. Sprung, H. Wu, and J. Martorell, Am. J. Phys. **61**, 1118 (1993).

[19] M. G. Rozman, P. Reineker, and R. Tehver, Phys. Lett. A **187**, 127 (1994).

[20] P. Pereyra, J. Math. Phys. **36**, 1166 (1995); P. A. Mello and J. P. Pichard, J. Phys. I **1**, 493 (1991).

[21] P. Pereyra, J. Phys. A **31**, 4521 (1998).

[22] P. Pereyra, Phys. Rev. Lett. **84**, 1772 (2000).

[23] L. M. Kahn, Phys. Rev. B **53**, 1429 (1996).

[24] H. M. James, Phys. Rev. **76**, 1602 (1949).
[25] P. Erdös and R. C. Herndon, Adv. Phys. **31**, 63 (1982).
[26] P. A. Mello, P. Pereyra, and N. Kumar, Ann. Phys. (N.Y.) **181**, 290 (1988); E. Merzbacher, *Quantum Mechanics* (Wiley, New York, 1970).
[27] J. M. Luttinger, Philips Res. Rep. **6**, 303 (1951).
[28] R. E. Borland, Proc. R. Soc. London, Ser. A **84**, 926 (1961).
[29] Philip F. Bagwell, Phys. Rev. B **41**, 10 354 (1990).
[30] H. A. Kramers, Physica (Amsterdam) **2**, 483 (1935).
[31] I. M. Gelfand *et al.*, Adv. Math. **112**, 218 (1995).
[32] P. Pereyra (unpublished).
[33] To describe the physics of thick-layer systems, it is useful but not necessary to use the effective mass approximation.
[34] R. de L. Kronig and W. G. Penney, Proc. R. Soc. London, Ser. A **130**, 499 (1931).
[35] A. M. Steinberg, P. G. Kwiat, and R. Y. Chiao, Phys. Rev. Lett. **71**, 708 (1993).
[36] J. L. Cardoso, P. Pereyra, and A. Anzaldo-Meneses, Phys. Rev. B **63**, 153301 (2001).
[37] F. García-Moliner and V. R. Velasco, *Theory of Single and Multiple Interfaces* (World Scientific, Singapore, 1992).
[38] Stephen Barnett, *Matrices, Methods and Applications* (Oxford University Press, Oxford, 1990).